ELSEVIER

# Plio–Quaternary sedimentation processes and neotectonics of the northern continental margin of the South China Sea

T. Lüdmann[a],[*], How Kin Wong[a], Pinxian Wang[b]

[a]*Institute of Biogeochemistry and Marine Chemistry, University of Hamburg, Bundesstrasse 55, D-20146 Hamburg, Germany*
[b]*Laboratory of Marine Geology, Tongji University, Shanghai 200092, People's Republic of China*

## Abstract

Analyses of over 6600 km of reflection seismic profiles on the northern continental margin of the South China Sea permit the recognition of four Quaternary high-frequency type 1 sequences of the 4th order, deposited during the past ca. 690 kyr. At the present-day shelf edge, only lowstand systems tracts characterised by a prograding clinoformal internal reflection pattern are preserved. The prograding complexes can be considered as regressive units accumulated during relative sea-level falls. They exhibit internal discontinuities which might point to minor sea-level fluctuations of the 5th order. A preliminary regional relative sea-level curve for the past 630 kyr is established using the present positions of the delta fronts mapped. The neotectonics curve derived by subtracting eustatic sea-level changes from the relative sea-level curve shows that the depths of the delta fronts today are controlled primarily by regional tectonic movements and the global sea-level.

Our seismo-stratigraphic interpretation documents that the area off Hong Kong and around the Dongsha Islands experienced two uplift episodes during the past 5 ma, namely at the Miocene/Pliocene boundary and at the end of the lower Middle Pleistocene, respectively. These uplift events which are centred on the Dongsha Rise led to its subaerial exposure and to the erosion of the Pliocene and most of the Pleistocene strata. The change from thermal subsidence of the continental margin initiated at the end of the drift phase to the phase of magmato-tectonic uplift was caused by a reorientation of the tectonic regime.

The Recent depositional environment on the northern continental margin of the South China Sea is dominated by sediment accumulation within the inner shelf and the Zhujiang (Pearl River) estuary. The outer shelf and upper slope, especially around the Dongsha Islands, are characterised by bypass of terrigenous material.

The sedimentary column in the deepsea basin has a thickness of more than 2 km and comprises 14 depositional units starting with terrestrial rift deposits. It overlies oceanic as well as transitional crust. © 2001 Elsevier Science B.V. All rights reserved.

*Keywords*: Sedimentation processes; Neotectonics; Seismic sequences; Forced regression; South China Sea

## 1. Introduction

The South China Sea is bounded to the west by Vietnam, to the north by southeastern China and Taiwan Island, to the east by the Philippine arc and to the south by Malaysia and Indonesia (Fig. 1). It has a maximum water depth of over 4000 m. Gravimetric studies, reflection seismic data, magnetic anomalies and rock samples from the seafloor have confirmed the oceanic character of its central part (Ludwig et al., 1979; Taylor and Hayes, 1980; 1983). The northern margin of the South China Sea has been the

* Corresponding author. Fax: +40-428-386-3447.
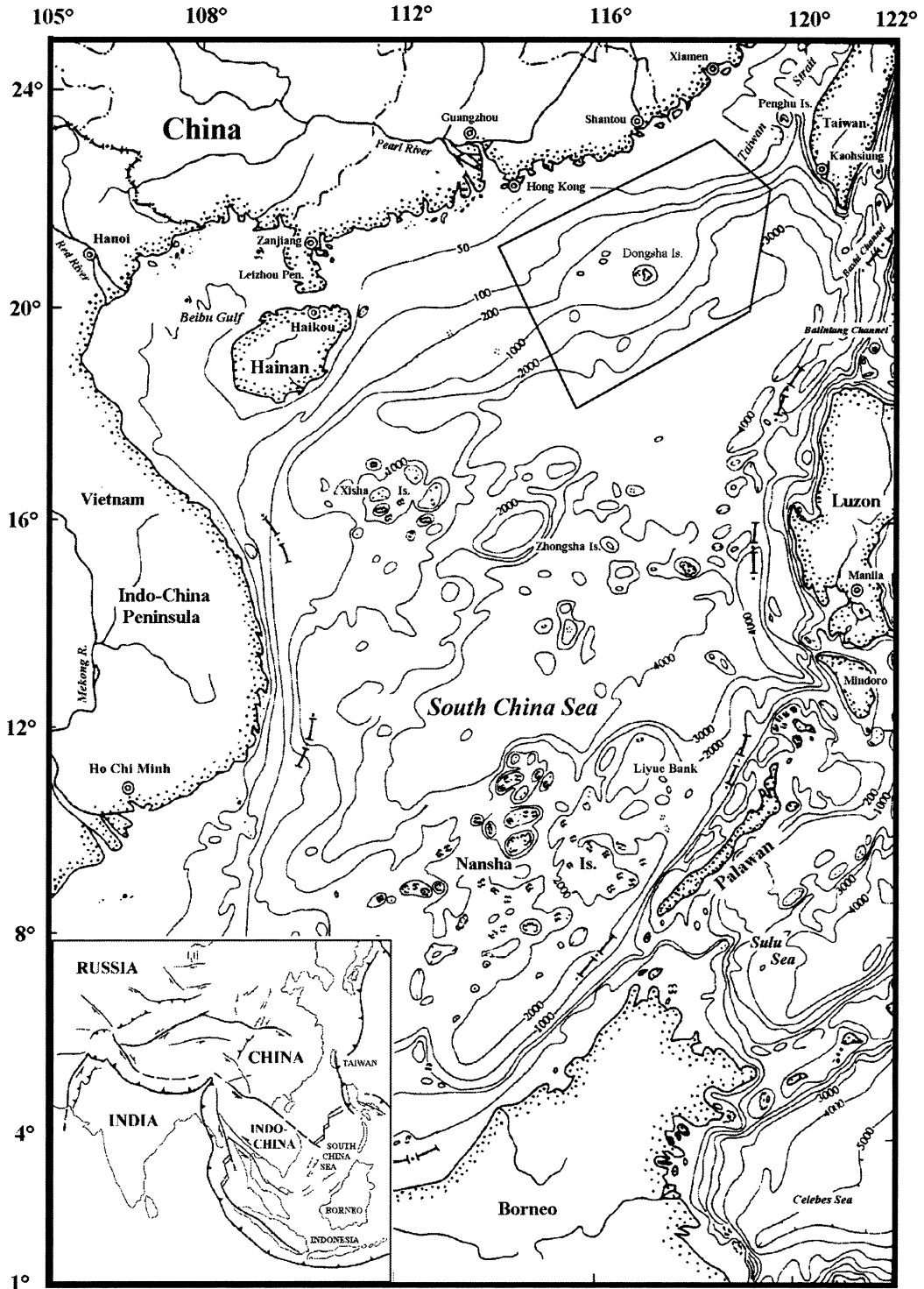  *E-mail address:* luedmann@geowiss.uni-hamburg.de
(T. Lüdmann).

Fig. 1. Map of the South China Sea showing the location of the study area (pentagon). Insert shows the schematic geotectonic framework.

subject of detailed investigations for many years. In the following, only selected comprehensive studies are mentioned. The basement structure and tectonic regime have been intensively investigated (Taylor and Hayes, 1980; 1983; Pautot et al., 1986; Li and Rao, 1994; Lee and Lawver, 1995; Spangler-Nissen et al., 1995; Lüdmann and Wong, 1999). The same is also true for the oil-bearing pre-Pliocene strata (Cai, 1987; Hu and Xie, 1987; Chen and Hu, 1989; Fulthrope and Schlanger, 1989; Guong et al. 1989; Erlich et al., 1990; Feng et al., 1992; Tyrrell and Christian, 1992). Although general overviews on Cenozoic sedimentation in the South China Sea exist (Wu, 1988; Wu, 1994), detailed studies on the post-Miocene sedimentation processes are still not yet available (Damuth, 1980; Niino and Emery, 1961; Feng et al. 1988; Li et al., 1991; Schönfeld and Kudrass, 1993; Xue et al., 1996). Recent studies have concentrated on the response of the West Pacific marginal seas to global climatic change (Wang et al., 1996). Of particular importance in this respect is the East Asian monsoon system which exercises a decisive control on the hydrography and sedimentation processes of the South China Sea (Sarnthein and Wang, 1999). In 1999, five sites have been successfully drilled during ODP leg 184 on the northern continental margin of the South China Sea to investigate the monsoonal history of East Asia (Wang et al., 2000).

The sedimentation history of the northern South China Sea was dominated by terrestrial deposition of the Shenhu, Wenchang and Enping formations during the rift phase (Table 1). Later, with the beginning of seafloor spreading, the sea encroached on the continental margin and a marine paleo-environment was established (Li, 1984; Wu, 1988; Guong et al., 1989; Feng et al., 1992). Meanwhile, the continental margins surrounding the South China Sea have been the site of outbuilding of giant carbonate platforms and local reef growth (Wu, 1988; Wu, 1994; Chen and Hu, 1989; Chen et al., 1994). Subsequent to the drift phase, thermal subsidence of the continental margins terminated reef-building abruptly (Aquitanian to lower Burdigalian; Erlich et al., 1990), only in local areas has it persisted into Recent times. These reefs have been studied in detail, especially in the Pearl River Mouth Basin (Cai, 1987; Hu and Xie, 1987; Chen and Hu, 1989; Fulthrope and Schlanger, 1989; Erlich et al., 1990; Tyrrell and Christian, 1992).

Concomitant with the onset of the drift phase (32 Ma), a large deltaic system of the paleo-Zhujiang (Pearl River) developed on the northern continental margin of the South China Sea (Guong et al., 1989; Chen et al., 1994). It exhibits a retrograding aggradational onlap pattern which indicates a continuous sea-level rise accompanied by a successive landward retreat of the depocenter (Chen et al., 1994). Since the Pliocene, this style of sedimentation has changed to an overall forestepping of the deltaic system.
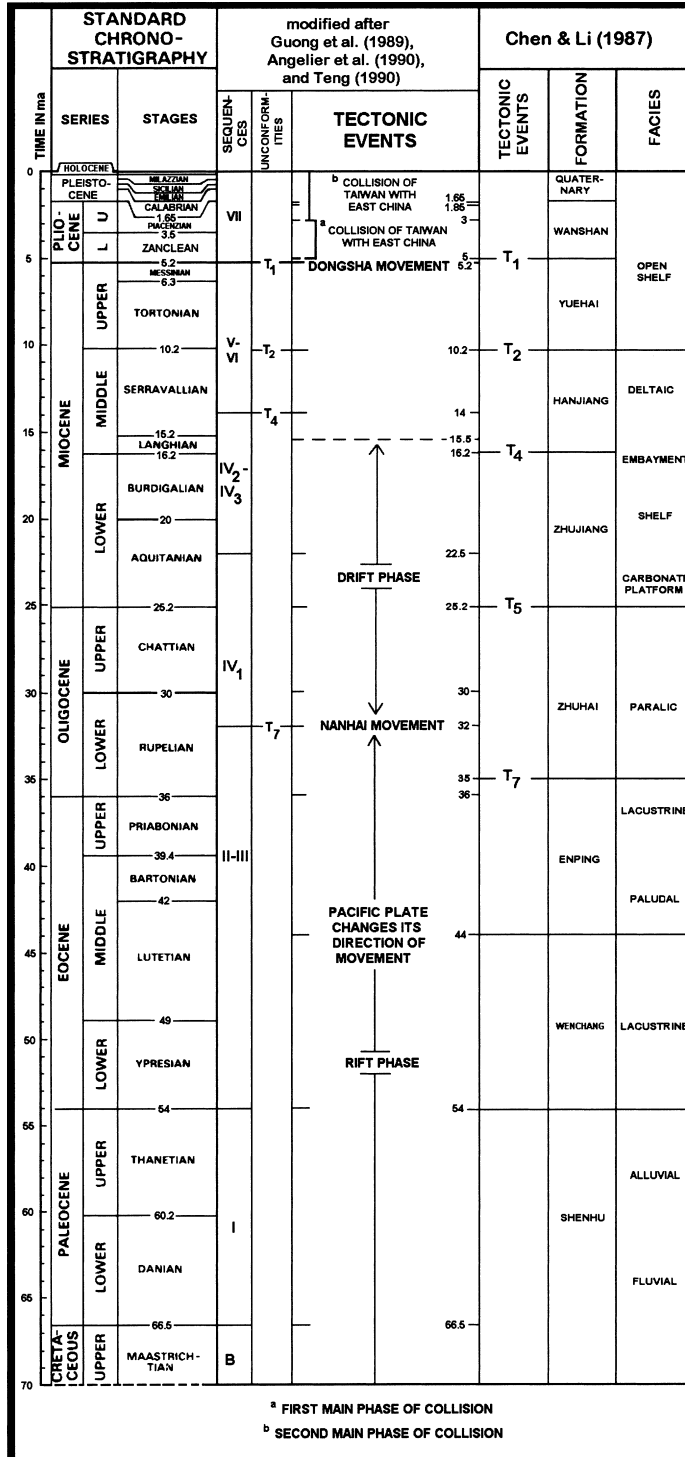
The main sediment source within the study area is the Pearl River (Fig. 1). At present, it discharges approximately $300 \times 10^9 \, m^3$ of water and $90 \times 10^6$ tons of sediment annually into its estuary (Gu et al., 1990). The delta progrades at an average rate of 50–60 m/yr and a maximum of 100 m/yr (Huang and Song, 1981). The water circulation pattern within the South China Sea is controlled by monsoons as well as the Kuroshio which flows northwards year-round along the east coasts of the Philippines and Taiwan Island towards Japan. Along its way, part of the flow enters the South China Sea through the Bashi Strait, where it splits into two branches, one flowing into the East China Sea through the Taiwan Strait and the other forming a counter-clockwise current within the South China Sea. The surface currents are driven by monsoons, which redirect the water masses to the northeast in the summer and to the southwest during the winter (Niino and Emery, 1961; Guan, 1993; Shaw and Chao, 1994; Wang et al., 1995).

Fig. 2 is a block diagram of the bathymetry of the study area compiled from Hydrosweep and Seabeam data collected by the R/V *Sonne* as well as from charts of the British Hydrographic Office (1986) and SCSIO (1986). It shows a distinct, broad continental shelf with the 200 m isobath extending more than 200 km off the Chinese coast. In the vicinity of the Dongsha Islands between 200 and 600 m water depth, the shelf edge is replaced by a plateau elongated NE–SW. This plateau has a quasi-rhombohedral shape and the Dongsha Islands are situated where the plateau is broadest near its southeastern margin. The Dongsha Islands form an atoll which emerges only a few tens of meters above sea-level. To the southwest, the upper slope is smooth and gently seaward-dipping. In contrast, it is dominated by a more-or-less rugged relief to the northeast.

The present paper focuses on the reconstruction of the less known post-Miocene geological evolution of

Table 1
Stratigraphy, sequences, unconformities and tectonic events of the Pearl River Mouth Basin

| TIME IN ma | SERIES | STAGES | SEQUENCES | UNCONFORMITIES | TECTONIC EVENTS (modified after Guong et al. (1989), Angelier et al. (1990), and Teng (1990)) | TECTONIC EVENTS (Chen & Li 1987) | FORMATION | FACIES |
|---|---|---|---|---|---|---|---|---|
| 0 | HOLOCENE | | | | | | QUATERNARY | |
| | PLEISTOCENE | MILAZZIAN SICILIAN EMILIAN | VII | | b COLLISION OF TAIWAN WITH EAST CHINA 1.65 1.96 | | | |
| | PLIO-CENE U | CALABRIAN 1.65 PIACENZIAN 3.5 | VII | | 3 | | WANSHAN | |
| 5 | PLIO-CENE L | ZANCLEAN 5.2 | | T1 | a COLLISION OF TAIWAN WITH EAST CHINA 5 5.2 | T1 | | OPEN SHELF |
| | MIOCENE UPPER | MESSINIAN 6.3 TORTONIAN | V-VI | | DONGSHA MOVEMENT | | YUEHAI | |
| 10 | | 10.2 | V-VI | T2 | | T2 10.2 | | |
| | MIOCENE MIDDLE | SERRAVALLIAN | | T4 | | | HANJIANG | DELTAIC |
| 15 | | 15.2 LANGHIAN 16.2 | IV2-IV3 | | 14 15.5 16.2 | T4 | | EMBAYMENT |
| 20 | MIOCENE LOWER | BURDIGALIAN 20 | IV2-IV3 | | DRIFT PHASE | | ZHUJIANG | SHELF |
| | | AQUITANIAN | | | 22.5 | | | CARBONATE PLATFORM |
| 25 | | 25.2 | | | 25.2 | T5 | | |
| | OLIGOCENE UPPER | CHATTIAN | IV1 | | | | ZHUHAI | PARALIC |
| 30 | | 30 | IV1 | | 30 32 | | | |
| | OLIGOCENE LOWER | RUPELIAN | | T7 | NANHAI MOVEMENT | | | |
| 35 | | 36 | | | 35 36 | T7 | | |
| | EOCENE UPPER | PRIABONIAN 39.4 | II-III | | | | ENPING | LACUSTRINE |
| 40 | | BARTONIAN 42 | II-III | | | | | PALUDAL |
| 45 | EOCENE MIDDLE | LUTETIAN | | | PACIFIC PLATE CHANGES ITS DIRECTION OF MOVEMENT 44 | | | |
| | | 49 | | | | | WENCHANG | LACUSTRINE |
| 50 | EOCENE LOWER | YPRESIAN | | | RIFT PHASE | | | |
| 55 | | 54 | | | 54 | | | |
| | PALEOCENE UPPER | THANETIAN | I | | | | | ALLUVIAL |
| 60 | | 60.2 | I | | | | SHENHU | |
| 65 | PALEOCENE LOWER | DANIAN | | | | | | FLUVIAL |
| | CRETACEOUS UPPER | 66.5 MAASTRICHTIAN | B | | 66.5 | | | |
| 70 | | | | | | | | |

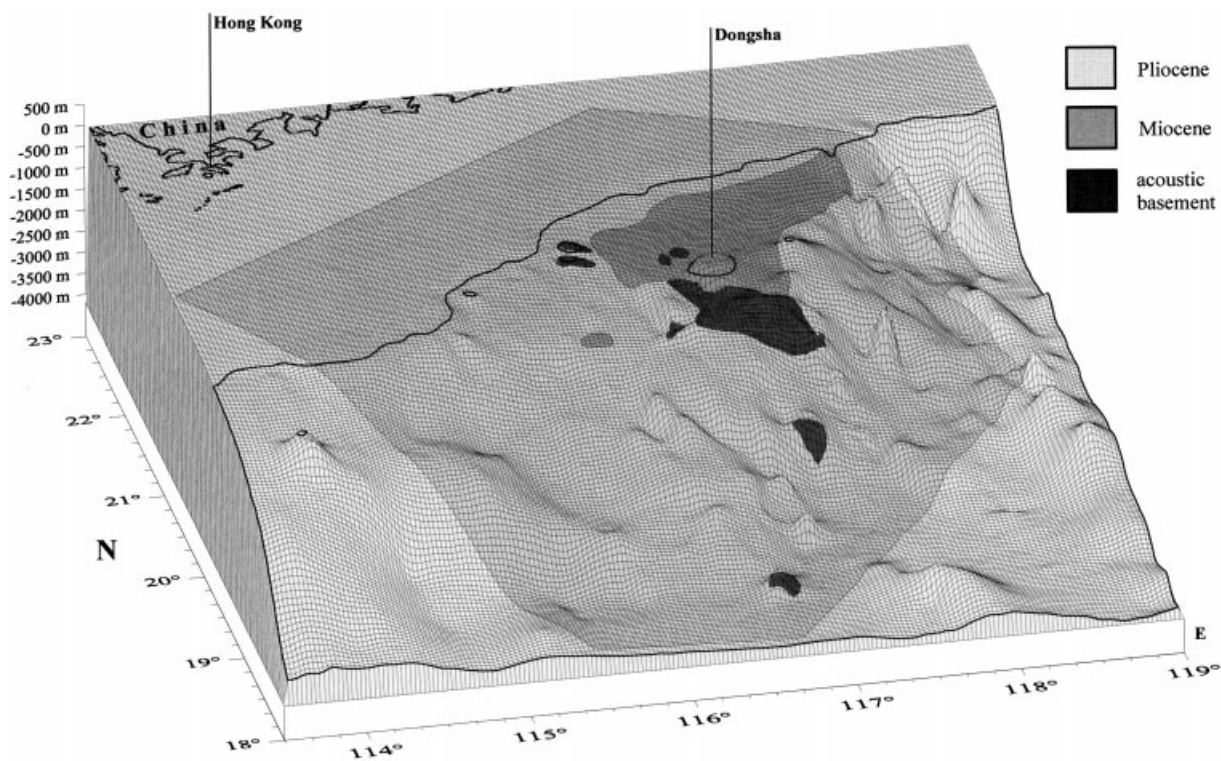a FIRST MAIN PHASE OF COLLISION

b SECOND MAIN PHASE OF COLLISION

Fig. 2. Three-dimensional diagram of the seafloor relief of the study area. Overlay shows the distribution of geologic formations after backstripping of the Quaternary section.

the northern South China Sea. The study area is located on the continental margin off Hong Kong. It extends between the Dongsha Islands and Taiwan (Fig. 1) and occupies an area of about 190,000 km². Reflection seismic profiles covering this study area are correlated with borehole data and box grab samples to elucidate the post-Miocene depo-environment (Fig. 3).

## 2. Methods

During three cruises aboard the German research vessel *Sonne* (SO-50B, 1987; SO-72A, 1990 and SO-95, 1994; Fig. 3), more than 6600 km of multi-channel reflection seismic data and high-resolution 3.5 kHz echograms as well as a number of box cores have been collected. During cruise SO-95, the seismic equipment used consisted of a GECO-PRAKLA mini-streamer (active length 100 m) and three GECO-PRAKLA air guns (total volume 5 l). The seismic data

were recorded digitally and later processed with a commercial software package. During the earlier cruises SO-50B and SO-72A, only an older analog system with online profile printout was available. Post-cruise data processing of these older lines to remove the effect of the bubble pulse and multiples was therefore not possible.

The basis of our seismo-stratigraphic interpretation is the lithostratigraphy of the wells LH 11-1-1A (Tyrrell and Christian, 1992), Zhu 2, Zhu 5 and Panyu 16-1-1 (Fig. 3, Table 2), together with p-wave velocities from sonobuoy stations (Fig. 3, Table 3) as well as from wire-line logs at the ODP sites (1144–1148, see Fig. 3) (Wang et al., 2000). On the Dongsha Rise, 87 m of Plio-/Pleistocene marine siltstones/mudstones with thin carbonate interbeds and 798 m of middle to upper Miocene marine mudstones and siltstones have been drilled (drill hole LH 11-1-1A, Fig. 3). The underlying layers consist of 476 m of porous lower Miocene carbonates (Zhujiang carbonate) which are made up of an
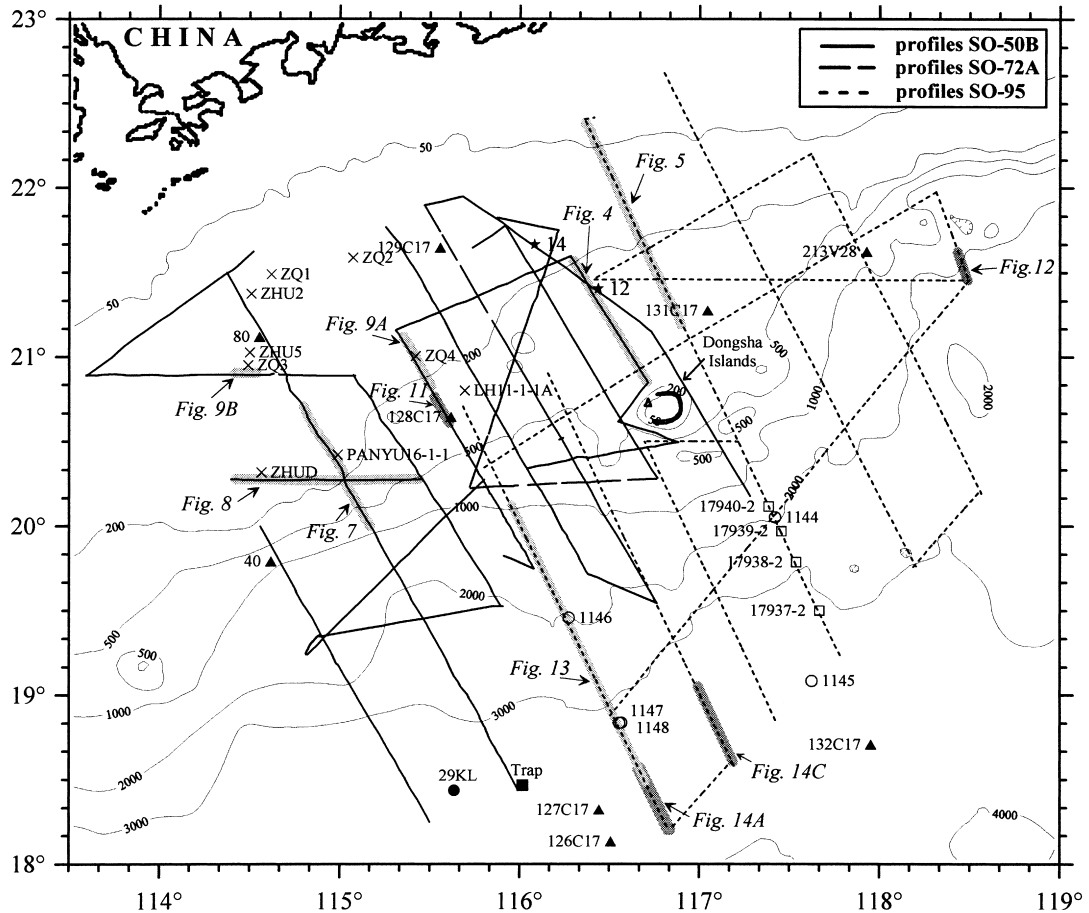
Fig. 3. Location of profiles obtained during cruises of the R/V *Sonne* in 1987 (SO-50B), 1990 (SO-72A) and 1994 (SO-95). Profiles presented in this paper are shadowed and labelled. Filled triangles: sonobuoy stations (Ludwig et al., 1979; Li, 1984); crosses: wells (LH11-1-1A: Tyrrell and Christian, 1992: ZHU2, ZHU3 and PY16-1: Guangzhou Marine Geological Survey of the Ministry of Geology and Mineral Resourses PRC, unpubl. data; ZQ1-4: Xue et al., 1996); filled square: sediment trap location (water depth 3350 m); filled circle: location of sediment core station 29 KL, cruise SO-50B, water depth 3766 m; filled stars: box grab stations (Wiesner, 1993); open circles: ODP sites (Wang et al., 2000); open squares: sediment core locations from cruise SO-95 (Wang et al., 1999).

upper unit in a bank and platform facies and a lower unit of fine-grained chalky limestones in a low-energy platform facies. This is in turn underlain by 149 m of porous upper Oligocene to lower Miocene quartz sandstones (Zhuhai sandstone) which overlie the Mesozoic granitic basement.

## 3. Seismic sequences, seismic facies and their lithostratigraphic correlation

For the Quaternary, a set of hitherto undocumented

Table 2
Thickness in meters of the Neogene-Quaternary succession of selected exploration wells from the northern South China Sea (see Fig. 3 for well locations)

| Epochs | | Zhu 2 | Zhu 5 | Panyu 16-1-1 | LH 11-1-1A |
|---|---|---|---|---|---|
| Quaternary | | 196 | 209 | 209.8 | |
| Pliocene | | 246.5 | 268.5 | 187.5 | 87 |
| Miocene | U | 356.5 | 355 | 360.5 | |
| | M | 679.5 | 673.5 | 732 | 798 |
| | L | 621.5 | 574 | 508.2 | 1361 |

Table 3

Sonobuoy velocities in km/s from the northern South China Sea: (A) after Ludwig et al. (1979); and (B) after Li (1984) (see Fig. 3 for locations of sonobuoy stations)

**A**

| Sonobuoy | V1 | V2 | V3 | V4 | V5 | V6 | V7 |
|---|---|---|---|---|---|---|---|
| 126C17 | 1.73 | 2.07 | 2.44 | 2.49 | 5.00 | 6.20 | 6.70 |
| 127C17 | 1.84 | 2.04 | 2.92 | 5.10 | | | |
| 128C17 | 2.00 | 2.60 | 3.05 | 5.10 | 6.10 | 7.20 | |
| 129C17 | 2.05 | 2.40 | 2.80 | 3.20 | | | |
| 131C17 | 2.20 | 4.40 | | | | | |
| 133C17 | 1.92 | 2.68 | 2.71 | 5.00 | 5.55 | | |
| 213V28 | 1.80 | 2.30 | 2.95 | 4.70 | 5.45 | 6.05 | |

**B**

| Sonobouy | V1 | V2 | V3 | V4 | V5 | V6 |
|---|---|---|---|---|---|---|
| 80 | 1.6, 1.85 | 2.2, 2.45, 2.75 | 3.0, 3.5 | 3.9 | 4.2, 4.6 | 7.05 |
| 40 | 2.0 | 2.3, 2.65, 2.95 | 3.25, 3.5 | 3.9 | 4.3 | 5.25 |
| | Quaternary-Pliocene | upper Miocene | middle Miocene | lower Miocene | Oligocene | Cretaceous |

high-frequency 4th order sequences was recognised in the Dongsha region. The established stratigraphy within the Pearl River Mouth Basin is based predominantly on the recognition of 2nd to 3rd order sequences and will be presented briefly below. Because of inconsistencies in the numbering of the sequences and unconformities within the Pearl River Mouth Basin (e.g. the middle Oligocene regional breakup unconformity is named $T_7$ as well as $T_6$ in the literature), we shall adhere to the convention of Guong et al. (1989) for the sequence stratigraphy and lithostratigraphy and to that of Chen and Li (1987) for the unconformities.

Two types of acoustic basement can be distinguished within the study area (Table 4). The first type ($B_{sed}$) is characterised by strong, hyperbolic surface reflections, the amplitude of which quickly diminishes with increasing penetration. Parallel reflectors exist sporadically in the subsurface. This documents its sedimentary origin. The second type ($B_{ign}$) consists exclusively of strong hyperbolic reflections, the intensity of which slowly diminishes with increasing depth. Internal stratifications are absent. Examples are the oceanic crust and magmatic intrusions within the continental crust. Granites, diorites and quartz-porphyrites of Mesozoic (late Yenshanian movement) or Cenozoic age (rift phase) probably dominate the rock types.

The Enping, Wenchang and Shenhu formations (sequences I–III) consist seismically of subparallel, discontinuous reflectors of varying amplitude (Table 4). Their internal configuration is typical of nonmarine deposits. They occur as rift depression fill and comprise sandstones, siltstones and mudstones. Sandy conglomerates occur sporadically.

The Zhuhai formation (sequence $IV_1$) is characterised by chaotic, hyperbolic reflections with high amplitudes (Table 4) attributable to coarse, clastic fluvial-marine to coastal sediments which are probably erosional products of the elevated rift shoulders. Sequence $IV_2$, a lower Miocene sandstone, is seismically masked on the Dongsha Rise by carbonate rocks of the overlying sequence $IV_3$. The latter is marked by strong surface reflections of high continuity. The reef and platform carbonates are bounded at the top by a prominent unconformity ($T_4$). Sequences $IV_2$–$IV_3$ correspond to the Zhujiang formation.

Sequences V–VI, corresponding to the middle to upper Miocene Yuehai and Hanjiang formations by correlation (Table 4), consist of an interbedded series of siltstones, mudstones and sandstones with intercalations of carbonates and dolomites. Seismically, they are represented by continuous parallel reflectors with medium amplitude. These Miocene deposits are separated from the Pliocene by a major erosional unconformity ($T_1$; Table 1).

The Pliocene Wanshan formation and the Quaternary (sequence VII) consist of continuous, parallel reflectors of high to medium amplitude (Table 4). In these deposits, clay predominates over silt and sand. A seismo-stratigraphic interpretation of our seismic profiles permits the recognition of five high-frequency

Table 4
Summary of the seismic facies and stratigraphic correlations of the seismic sequences within the study area. The revised unconformity ages are also shown
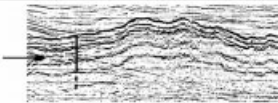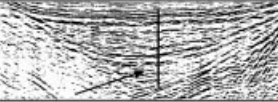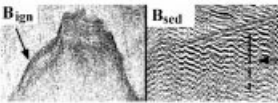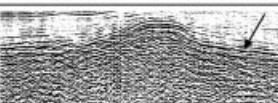
| Sequence | Formation | System | Internal Reflection Configuration | Frequency | Amplitude | Continuity | |
|---|---|---|---|---|---|---|---|
| VII $T_0$ $T_1$ | Quaternary, Wanshan | Quaternary– Pliocene | parallel | slightly variable | medium | intermediate |  |
| V-VI $T_2$ $T_4$ | Yuehai, Hanjiang | upper Miocene– late-middle Miocene | parallel | uniform | medium | high |  |
| $IV_2$-$IV_3$ | Zhujiang | mid-middle Miocene– mid-lower Miocene | parallel | low | high | high |  |
| $IV_1$ $T_7$ | Zhuhai | early lower Miocene– upper Oligocene | hyperbolic to chaotic | variable | high | high |  |
| I-III | Shenhu, Wenchang, Enping | lower Oligocene– Paleocene | subparallel | highly variable | variable | discontinuous |  |
| continental basement | – | Cretaceous– Triassic | $B_{ign}$: hyperbolic to chaotic $B_{sed}$: parallel to subparallel | low | high | high laterally, low vertically |  |
| oceanic basement | – | lower Miocene– upper Oligocene | hyperbolic | low | high | high laterally and vertically |  |

Table 5
Regressive seismic units (E, D, B and A, light gray) and transgressive unit (C, dark gray) recognised on the northern continental margin of the South China Sea off Hong Kong; SPECMAP δ¹⁸O isotopic record from Imbrie et al. (1993); relative sea-level and neotectonics curves derived from our seismic data; and relative sea-level curve from Xue et al. (1996) determined by bio- and lithofacies data from the ZQ 3 well (see Fig. 3 for well location) as well as from seismic profiles

| Symbol | Stratigraphy | | Age (ka BP) | Sequence Stratigraphy | SPECMAP δ¹⁸O ‰ | Neotectonics subsidence (m) uplift | Computed Relative Sea-Level (m) | Relative Sea-Level from ZQ3 (after Xue et al., 1996) |
|---|---|---|---|---|---|---|---|---|
| Q4 | Holocene | | | | | | | Terrestrial / Coastal / Inner Shelf / Outer Shelf |
| Q33 | Late Pleistocene | U | | A | 2 | | | |
| Q32 | | M | | | 4 | | | |
| Q31 | | L | 100 | 1 | 5 | | | |
| Q23 | | U | 200 | B 2 | 6, 7 | | | |
| Q22 | Middle Pleistocene | M | 300 | | 8, 9 | | | |
| | | | 400 | | 10, 11, 12 | | | |
| Q21 | | L | 500 | ? 2 C D 3 | 13, 14, 15 | | | |
| | | | 600 | | 16 | | | |
| | | | 700 | E ? | 17, 18 | | | |

Neotectonics scale: −200, −150, −100, −50, 0
Computed Relative Sea-Level scale (m): −300, −250, −200, −150, −100, −50, 0
SPECMAP scale: 3.2, 3.4, 3.6, 3.8, 4.0, 4.2, 4.4, 4.6, 4.8, 5.0, 5.2

4th order Quaternary seismic units (A–E, Table 5) on the continental shelf off Hong Kong.

## 4. Plio-Quaternary sedimentation processes

### 4.1. Shelf-upper slope province

Fig. 2 shows the geological formations of the study area with the Quaternary strata backstripped. In the eastern part of the margin which is dominated by the Dongsha Rise, Miocene deposits are unconformably overlain by a thin layer of Pleistocene sediments (in places only a few meters in thickness), whereas the western part is covered by thick Pliocene to Quaternary sediments (400–450 m, Table 2). Our data suggest that these two areas have evolved geologically differently over this time interval. Seismic reflection profile 16 (Fig. 4) located on the Dongsha Rise clearly demonstrates the absence of Pliocene strata and outcropping of the Miocene formation on the seafloor. High-resolution PARASOUND data west of line 16 (Fig. 5, profile 11) support this observation. The Pleistocene coarse relict sediments are marked by a strong
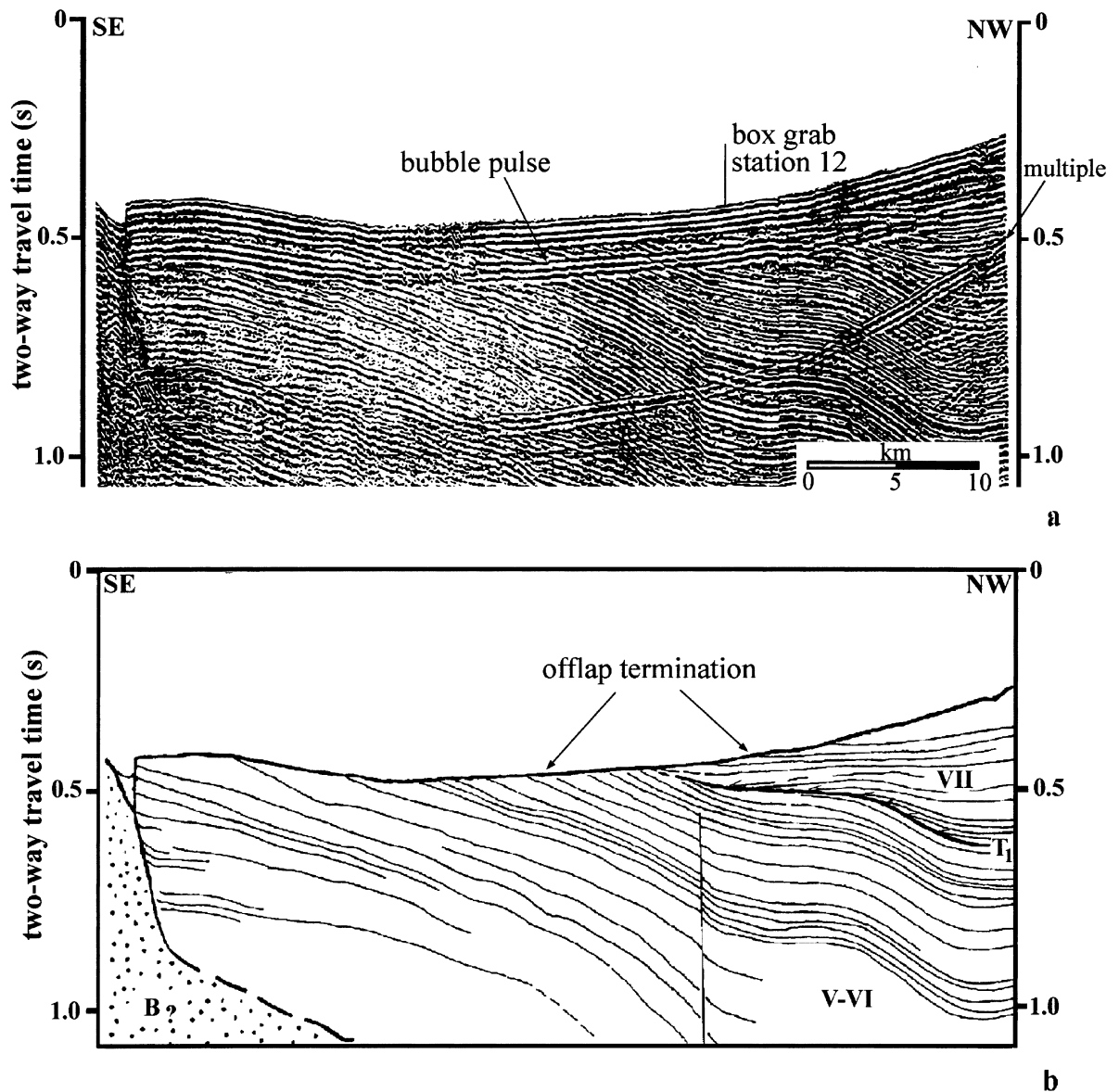
Fig. 4. (A) Part of reflection seismic profile 16 (SO-72A) on the Dongsha Rise and (B) interpretation. Roman numerals are sequence designations (see Tables 1 and 3). This profile shows outcropping of the Miocene formation (V–VI) which is unconformably overlain by Pliocene to Quaternary strata (VII). Offlap reflector terminations suggest that all formations have been truncated. See Fig. 3 for profile location.

continuous prolonged bottom echo with few or no subbottom reflections. On the upper slope (300–350 m water depth), they form a sheet-like body with a thickness of 10–15 m (Fig. 5). Their relict character has been confirmed by radiocarbon age dating (Fig. 6, facies type 3a and 3b; the sedimento-

logical facies 1–5 will be considered later). The underlying Miocene layers exhibit a sharp subbottom echo delineating a rough erosional surface. They are uplifted, dip to the north (Lüdmann and Wong, 1999) (Figs. 4 and 5), and outcrop at the seafloor at the SSE end of PARASOUND profile 11 (Fig. 5). This is the
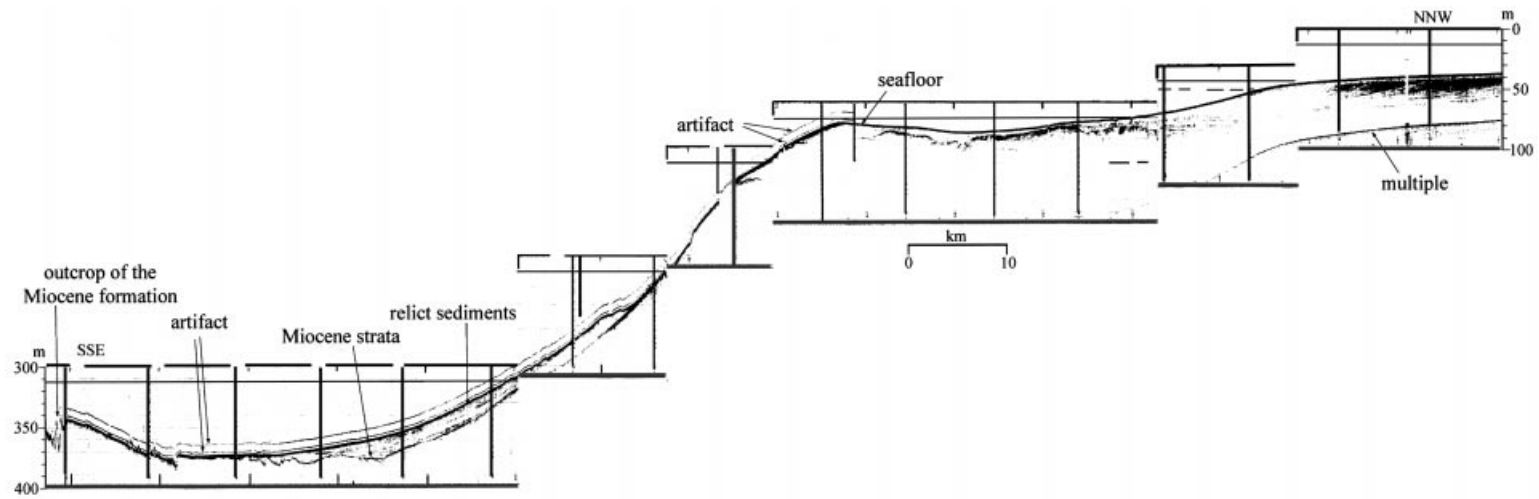
Fig. 5. PARASOUND profile 11 (SO-95) on the Dongsha Rise showing Miocene sediments bounded by an irregular erosional upper surface and unconformably overlain by relict sediments of late Pleistocene age. See Fig. 3 for profile location.
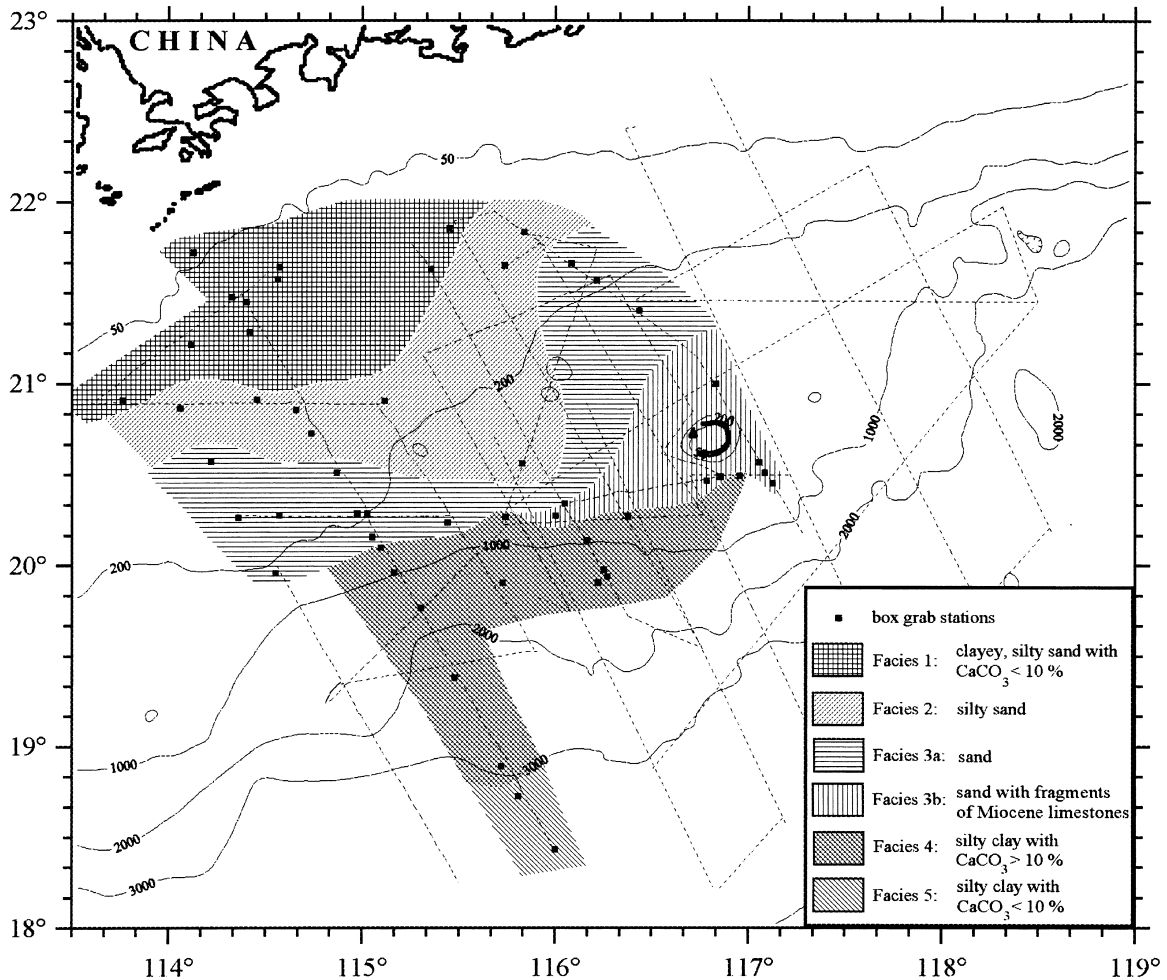
Fig. 6. Map showing the sedimentary facies distribution off Hong Kong deduced from bow grab samples of cruises SO-50B and SO-72A. After Wiesner, 1993.

result of two magmato-tectonic uplift events centred around the Dongsha Islands, namely at the Mio-/Pliocene boundary and within the lower Middle Pleistocene (Lüdmann and Wong, 1999). The uplift events with their subsequent subsidence phases in general, and the evolution of the area around the Dongsha Islands in particular will be discussed in Section 5.

### 4.1.1. Plio-Quaternary high-frequency seismic units

Interpretation of the reflection seismic profiles 1 and 8 (SO-50B) (Figs. 7 and 8) leads to the recognition of four type 1 sequences accumulated during the past ca. 690 kyr. They are of short duration and repre-

sent high-frequency sequences of the 4th order. We correlated our seismic data with the lithostratigaphy of the wells ZQ 3, ZQ 4 (Xue et al., 1996; Fig. 9), Zhu 2, Zhu 5 and Panyu 16-1-1 (Figs. 3 and 7 and Table 2) using p-wave velocities derived from sonobuoy measurements (Ludwig et al., 1979; Li, 1984; see Table 3). We note that these p-wave velocities are generally higher than those determined at the ODP sites which are in deeper waters (Wang et al., 2000). To bring the sonobuoy velocities into line with the ODP results, we reduced the sonobuoy velocities systematically by 15%.

Near the shelf edge off Hong Kong west of the

Dongsha Islands, four prograding wedges have been detected (A–E; Figs. 7 and 8). They are interpreted as progradational deltaic units because of their internal oblique-tangential seaward-dipping reflectors which generally terminate by toplap at the upper boundary and by downlap at the base (Sangree and Widmier, 1977). Unfortunately, terminations of the reflectors at the top of units A, B and D are partially masked by reverberation of the source signal and a bubble pulse. Only unit E on profile 8 shows a distinct toplap termination (Fig. 8) which suggests erosion of the upper part of the depositional unit, resulting in a lack of topset beds.

Within the prograding units A, B, D and E, internal discontinuities (ID) divide the wedges into smaller subunits (Figs. 7 and 8). The adjacent clinoforms terminate by onlap or downlap against these ID's at different dips on the two sides. The average dip angle lies between 0.5° and 2.5° with a maximum of 4°. The internal discontinuities may reflect minor sea-level fluctuations or delta lobe switching during progradation. Tesson et al. (1993, 1999) described internal discontinuities within their regional regressive seismic units in the Rhône delta. They named these IDs downward shift surfaces (dss) and ascribed their toeset erosion and the down-stepping geometry of their flat upper bounding surface to minor relative sea-level falls. Down-stepping of adjacent prograding units can also be inferred from our seismic data (Figs. 7 and 8). We suggest that in our study area both delta lobe switching and sea-level fluctuations might have played a role in creating the observed stacking pattern of the prograding complexes.

In addition to prograding clinoforms, we observed a unit with downlap terminations both up- and down-slope, resulting in a mound-like external geometry (C on Figs. 7 and 8). Since this unit overlies a prograding complex, it must have formed during the early phase of a sea-level rise. That it is ridge-like in form is suggested by correlation across profiles 1 and 8. Its internal reflections have high amplitudes, indicating that this unit consists of coarse material. We interpret this structure as a sand-ridge formed in the vicinity of the paleo-shoreline. Additional evidence may be found in the coastal facies assemblage of well ZQ 3 ca. 60 km landward of the sand-ridge mapped (Fig. 9). Comparable transgressive depositional systems have been described by Penland et al. (1988) from the

Mississippi delta as inner-shelf shoals (subaqueous barrier sands) as well as by Diaz and Maldonado (1990) from the Maresme continental shelf (Mediterranean Sea) as transgressive sand bodies.

Seismo-stratigraphic interpretations permit the determination of three types of bounding surfaces of different orders. Of the first order are master unconformities which separate sequences and are polygenetic in character (1–3, Figs. 7 and 8 and Table 5). They correspond to phases of transgression, regression and marine flooding. Unconformities of the second order are boundaries between systems tracts (1', 2'; Figs. 7 and 8) and occur within a single sequence. Internal discontinuities reflect unconformities of the third order and can be attributed to minor sea-level fluctuations during a period of a major relative sea-level fall.

We now consider the stratigraphic relationship between the seismic units and their depositional history. From profile 1, the depths of the offlap break of each delta front (1–4) below present-day sea-level were determined. By correlating the present locations of these delta fronts with the SPECMAP oxygen isotope record used as a proxy for the global sea-level curve (Imbrie et al., 1993), we obtained 4 points on the relative sea-level curve for the northern continental margin of the South China Sea. Since this curve is the sum of the eustatic and tectonic contributions to the regional relative sea-level fluctuations and since the eustatic component is known, the tectonic contribution could be computed. The results for the period ca. 630 ka (stage 14) to Recent times are shown in Table 5. These results, however, should be regarded only as a first approximation because of the paucity of data and of the fact that sediment loading, compaction and erosion have not been taken into account. For comparison, we also plotted the relative sea-level curve of Xue et al. (1996) deduced from borehole ZQ 3 (Fig. 3) for the past ca. 720 kyr using bio- and lithofacies and seismic data (Table 5).

Our sequence stratigraphic interpretation leads to the recognition of 5 systems tracts representing 4 lowstand wedges (regressive units A, B, D and E) and one transgressive unit (C) (Table 5, Figs. 7 and 8). The prograding clinoforms of the sediment wedges can be described as shelf-edge deltas deposited during periods of eustatic sea-level fall. The surfaces of these prograding complexes represent paleo-delta fronts
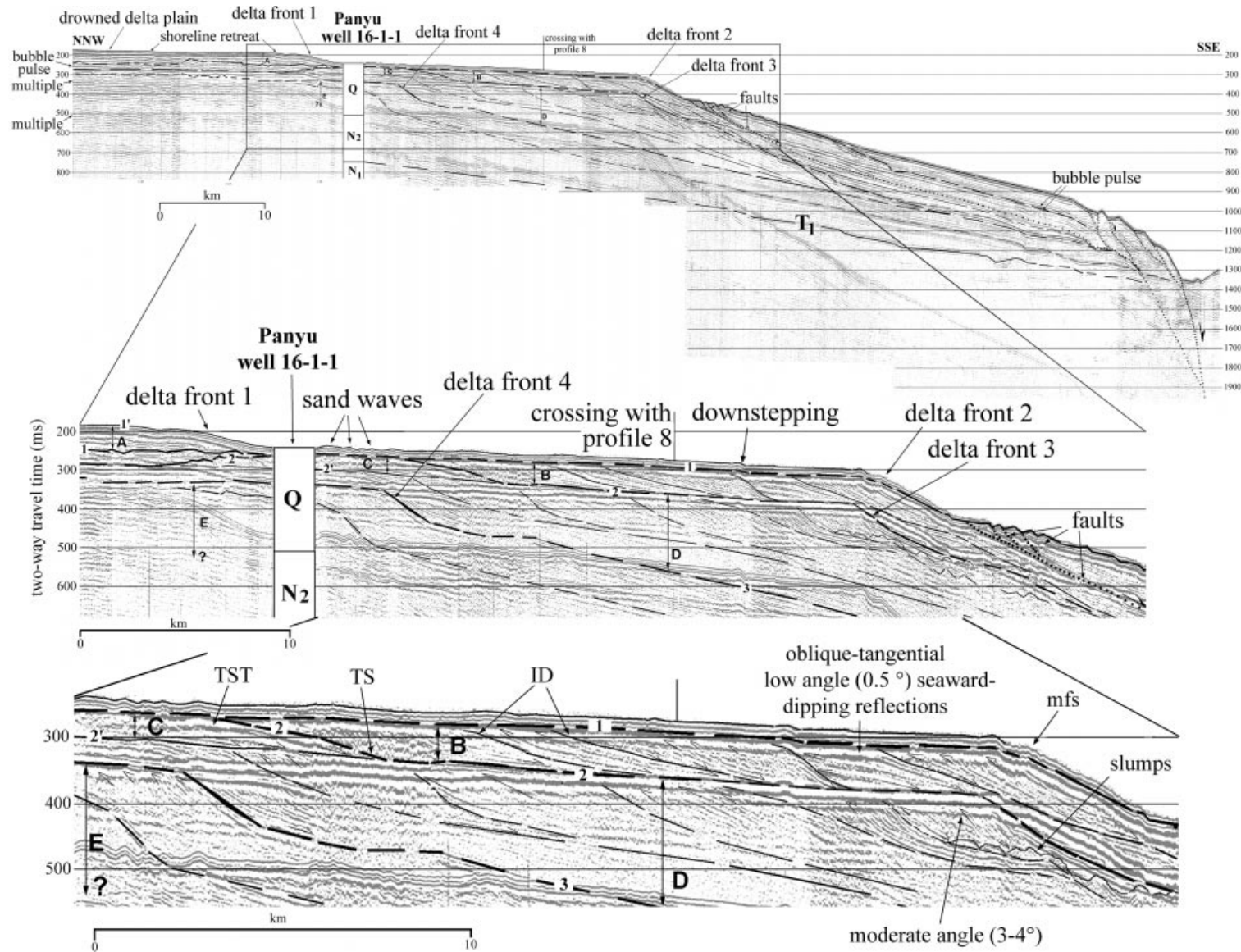
(Figs. 7 and 8). In classical sequence stratigraphy, a normal regression occurs during a relative sea-level rise when the terrigenous influx is high enough to over-compensate the added accommodation (Vail et al., 1977; Posamentier et al., 1988; Posamentier and Vail, 1988). The resulting prograding deposits are part of the transgressive systems tract. During a relative sea-level stillstand, a terrigenous influx also leads to a normal regression. In the case of a relative sea-level fall, accommodation is always reduced and a forced regression occurs (Posamentier et al., 1992). The regressive stratigraphic unit accumulated during a relative sea-level fall to early rise is the lowstand wedge for a continental margin with a shelf break (Posamentier and Vail, 1988). Sydow and Roberts (1994) postulated that the regressive wedge of the Alabama shelf was created during a relative sea-level fall and lowstand although formally they belong to a high-stand systems tract. Tesson et al. (1993, 1999) described regressive wedges from the Rhône delta (which they named regional prograding units) as depositional units accumulated during a relative sea-level fall.

We interpret the prograding delta wedges mapped near the present-day shelf break as lowstand wedges formed during forced regressions. During such an event, a rapid basinward shoreline migration resulted in a detachment of the regressive unit from the high-stand shoreline, the two being separated by a zone of sediment bypass and subaerial erosion. The prograding Pearl River delta of the Holocene is considered the result of a normal regression, with sediment influx exceeding the accommodation created by sea-level rise. Because longshore currents and wave action are strong (see Section 1), progradation of the Pearl River delta to the modern shelf edge seems unlikely. Although the SPECMAP curve shows that for the time period under consideration, the rate of eustatic sea-level fall was much lower than that of a eustatic sea-level rise, there are two factors that promoted a rapid regression during a sea-level fall. These factors are: (1) the gentle dip of the shelf (0.05–0.4°) for which a small relative sea-level fall already resulted

in a widespread exposure of the shelf; and (2) a continuous tectonic uplift of the continental margin since isotopic stage 14 (ca. 550 ka) which accentuated the effect of an eustatic sea-level fall.

The Panyu 16-1-1 well located close to profile 1 and with a drill depth of ca 2000 m penetrated into the lower Miocene (Fig. 7, Table 2). A correlation of the stratigraphy derived from this well with the seismic reflectors of profile 1 allows an extrapolation of the Mio-/Pliocene boundary (major unconformity $T_1$, Table 2) from the well location to the continental slope. Because the signal weakens in the deeper part of the seismic section and the multiples exercise a masking effect, the sequences between $T_1$ and the prograding complex E (delta front 4) as well as the lower boundary of E cannot be clearly distinguished (Figs. 7 and 8). Despite these difficulties, the offlap break of the complex E lying approximately 277 m below the present-day sea level may be interpreted as the delta front formed ca. 627 ka during a relative sea level fall using the correlation with the SPECMAP curve already discussed (Table 5, Figs. 7 and 8). The magnitude of this fall was about the same as that during the Last Glacial Maximum (LGM), namely about 130 m (Table 5; Emery et al., 1970; Feng et al., 1988; Schönfeld and Kudrass, 1993).

Delta front 3 (prograding complex D; Figs. 7 and 8) in turn would correspond to the sea-level fall of isotope stage 14 (552 ka; Table 5). The top of this delta front lies at a present-day depth of ca. 287 m and was formed when the eustatic sea-level was ca. 96 m below present (Table 5) and when a flood plain environment occurred at the location of borehole ZQ 3 (Fig. 9). Thus, during the period 627–552 ka, the continental margin must have subsided about 44 m [(287-96)–(277-130) m] (see neotectonic curve, Table 5). This corresponds to a rate of 59 cm/ka. For comparison, Ru and Pigott (1986) determined a subsidence rate of ca. 3 cm/ka for the entire Quaternary at the borehole Zhu D close to our seismic profile 8 (see Fig. 3 for locations), a value considerably lower than our rate. This discrepancy can be explained by: (1) the rate of Ru and Pigott (1986) is an average for a

Fig. 7. Reflection seismic profile 1 (SO-50B). Note the four lowstand delta complexes (A, B, D and E) and the transgressive systems tract (C). Q, Quaternary; $N_2$, Pliocene; $N_1$, Miocene; ID, internal discontinuities; TST, transgressive systems tract; TS, transgressive surface; mfs, marine flooding surface. See Fig. 3 for profile location.
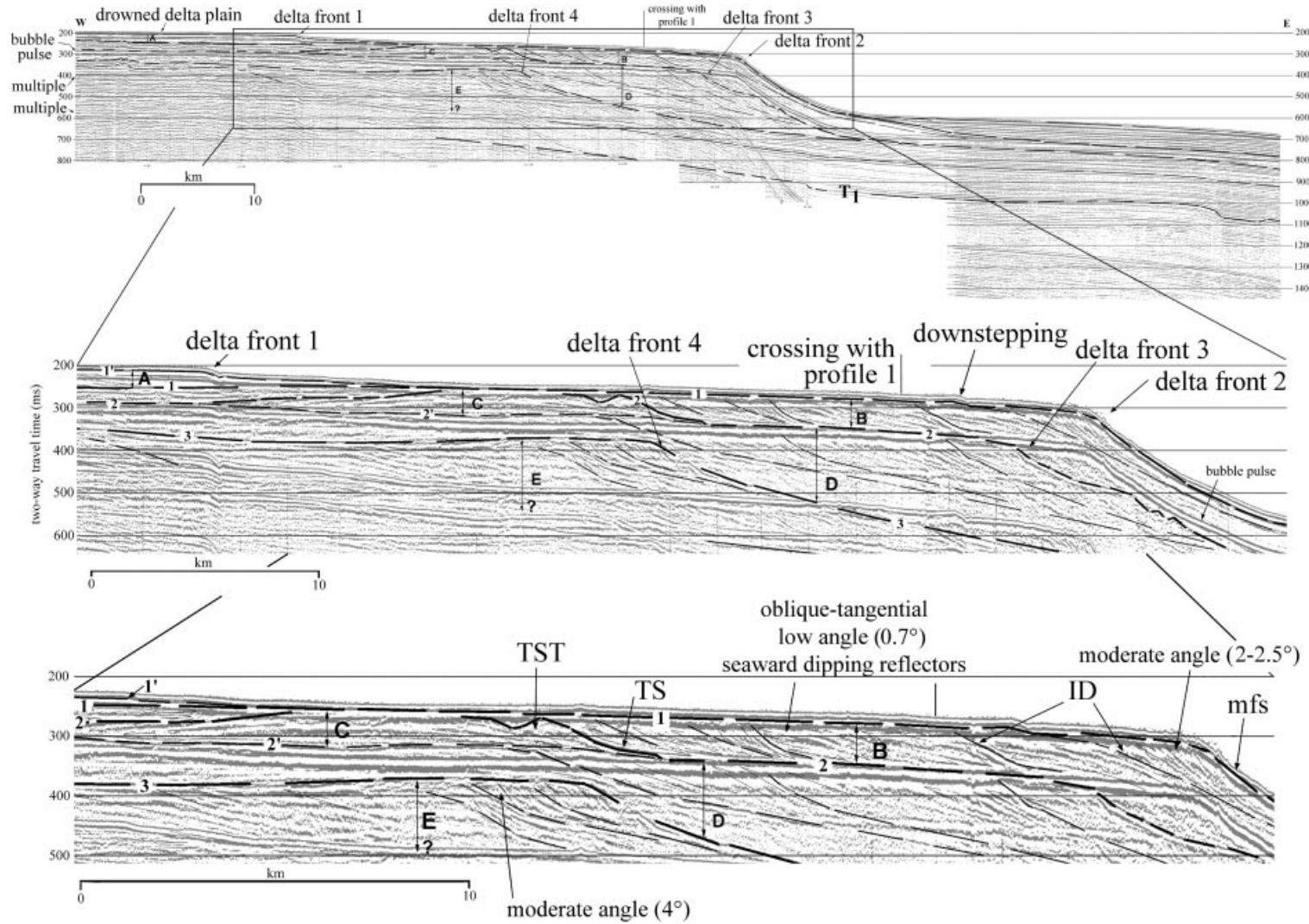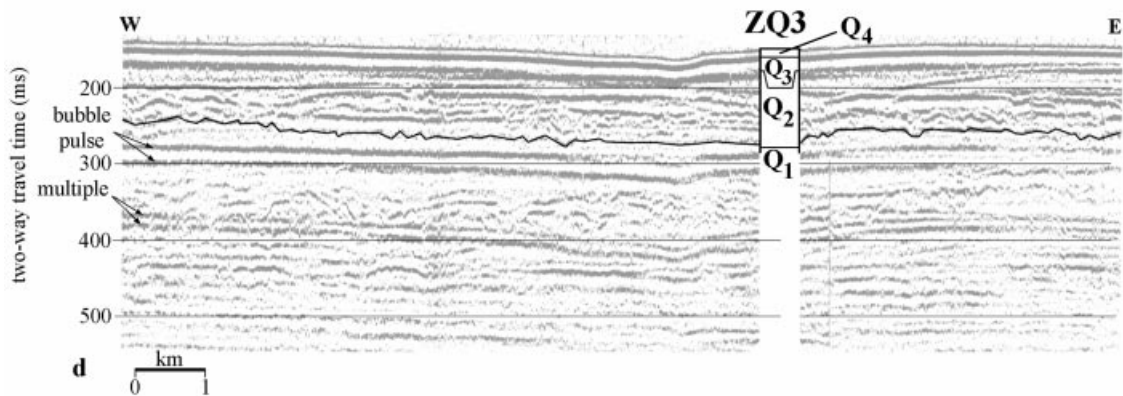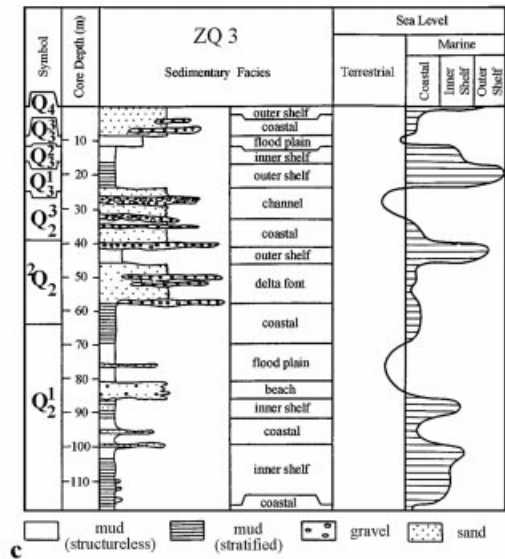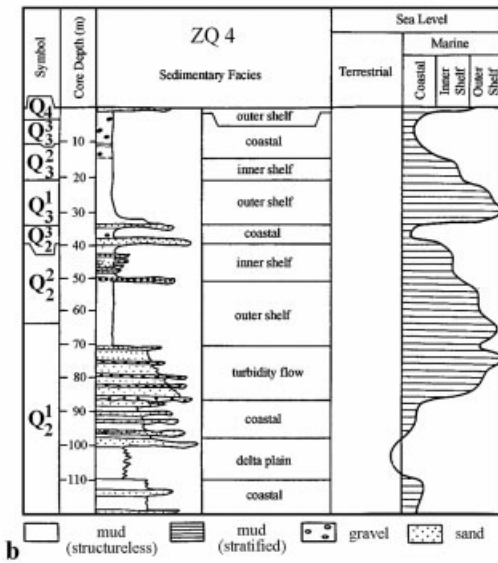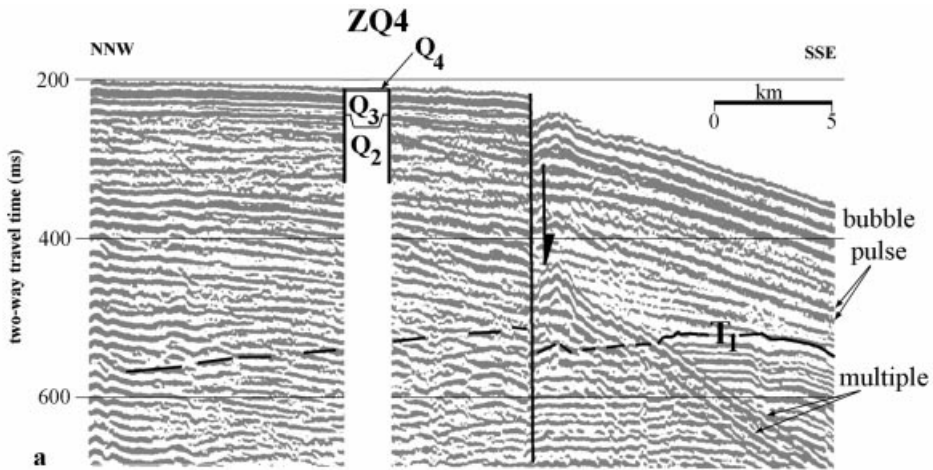
Fig. 8. Part of reflection seismic profile 8 (SO-50B). Note the four lowstand delta complexes (A, B, D and E) and the transgressive systems tract (C). Symbols same as in Fig. 7. See Fig. 3 for profile location.
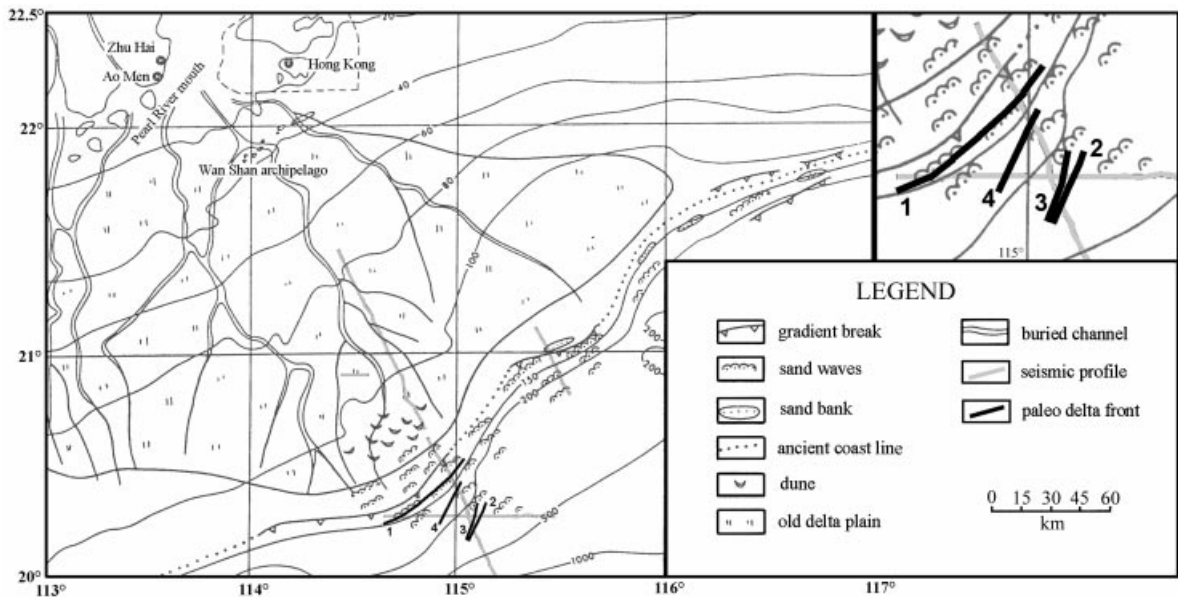
Fig. 10. Reconstruction of the paleo-depo-environment during the last glacial (after Feng and Shi, 1997). The paleo-delta front positions mapped are also shown (see also Figs. 7 and 8).

much larger time period (>1.8 Ma), so that rapid, short-duration tectonic events are "averaged out"; and (2) uplift events have not been recognised by Ru and Pigott (1986). The internal discontinuities of complex D may again be attributed to delta lobe switching or minor sea-level fluctuations. Slump deposits at the toe of the clinoforms of paleo-delta front 3 suggest that slope instabilities have led to mass wasting (Fig. 7). Such instabilities might have been triggered by tectonic events, high sedimentation rates and/or rapid delta progradation as attested to by the steep seaward-dipping reflectors. Complex D is bounded at its base by unconformity 3 and at its top by unconformity 2 (Figs. 7 and 8). It is in part overlain by the transgressive systems tract C which is represented by a mounded sand-ridge structure (Table 5). With the deposition of the sand-ridges, the coast shifted landward to the position of borehole ZQ 3 (Fig. 9). The deposits accumulated within the time interval between stages 12 and 8 are either not resolved by our seismic data or they have been eroded during the initial regression of stage 8. In particular, the highstand deposits are missing. They might have been deposited landward of our profiles far from the shelf edge as is the case today. Alternatively, the broad inner and middle shelf with a gentle dip of 0.05–0.4° could have been subaerial and therefore bypassed by sediments during a major sea-level fall. In this case, the highstand systems tract of the previous sea-level cycle could have been eroded.

Delta front 2 lies today at a water depth of ca. 221 m. It developed probably during the Saalian glacial (complex B, Figs. 7 and 8, Table 5) and prograded over the transgressive deposits (unit C) of the previous sequence. The incorporated cycles of the 5th order are expressed in our seismic data in the form of downstepping surfaces and internal discontinuities associated with short-lived rapid regional sea-level falls (Figs. 7 and 8). Unconformity 1 marks the upper boundary of unit B and the base of the Holocene

Fig. 9. (A) Part of reflection seismic profile 18 (SO-72A). $T_1$, Miocene/Pliocene unconformity. (B) Relative sea level curve and facies interpretation of well ZQ 4 (Xue et al., 1996). (C) Relative sea level curve and facies interpretation of well ZQ 3 (Xue et al., 1996). (D) Part of reflection seismic profile 3 (SO-50B). See Fig. 3 for profile and well locations.
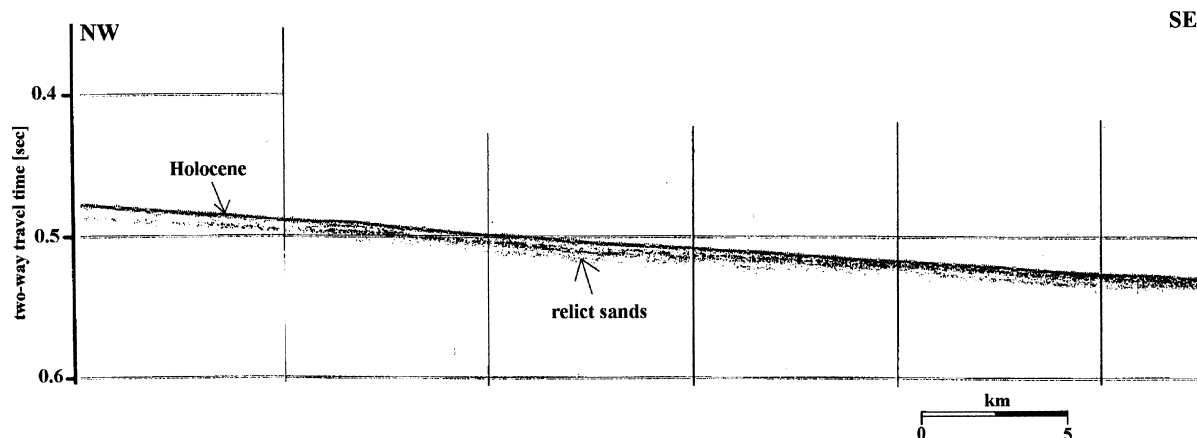
Fig. 11. Part of 3.5 kHz profile 18 (SO-72A). This profiles shows relict sediments (facies 3a and 3b, Fig. 6) on the upper slope (water depth ca. 370 m) ovelain by Holocene deposits. See Fig. 3 for profile location.

sequence. The inferred tectonics curve (Table 5) suggests that a phase of uplift of the continental margin at an average rate of ca. 16 cm/ka (552–135 ka) followed the subsidence of the time interval 627–552 ka.

The Weichselian glacial is marked by delta front 1 (prograding complex A) located today at a water depth of 145 m (Figs. 7 and 8). Since stage 6 (135 ka), the continental margin was uplifted about 84 m, corresponding to a rate of ca. 71 cm/ka (Table 5). On profile 1 (Fig. 7), Holocene paleo-shorelines can be interpreted to occur at water depths of 134 and 124 m. They exhibit an overall retrograding pattern implying phases of abrupt sea-level rise interrupted by phases of stillstand. While our profiles cross the distal part of this delta, well ZQ 3 is situated more landward and the sediment facies drilled points to a flood plain environment, namely the subaerial tidally-influenced part of the delta (Fig. 9). The well ZQ 4 in deeper waters shows for this time interval a coastal environment (Fig. 9). The minor sea-level fluctuations within this time period (Table 5) are not expressed on our seismic lines and may be beyond the resolution of our system. Fig. 10 shows our seismo-stratigraphic interpretation in relation to the reconstructed paleo-environment of the LGM published by Feng and Shi (1997). Their reconstruction is based on a large amount of core material and geophysical data collected during a five-year Chinese marine engineering program. Our interpretation is in good agreement with their reconstructed paleo-environment. For example, delta front 1

lies adjacent to the gradient break and the sand waves of Feng and Shi (1997) can be identified on our seismic profile 1 at the corresponding locations (Fig. 7). The positions of the pre-Weichselian delta fronts (2–4) are also shown in Fig. 10.

### 4.1.2. Holocene sedimentation processes

Fig. 6 shows the facies distribution of surface sediments determined from box grab samples of cruises SO-50B and SO-72A (Wiesner, 1993). Five facies regions were recognised: Facies 1 on the inner shelf may be attributed to the Pearl River. Facies 2 is represented by a mixture of recent and relict components and can be characterised as palimpsest (Wiesner, 1993). Facies 3 comprises relict sands and facies 4 and 5 are hemipelagic in origin. Correlatable with this sediment facies distribution is the echo-type distribution derived from our high-resolution PARASOUND and 3.5 kHz pinger profiles. It suggests that on the outer shelf, Holocene deposits are present only in paleo-channels. These channels reach 20 km in width and are filled with sediments of the Holocene sea-level rise (transgressive systems tract). Northwest of the Dongsha Islands, Holocene deposits can be traced to a water depth of 300 m where they terminate by downlap on Pleistocene relict sands (Fig. 11). These relict deposits have been sampled at box grab stations up to a water depth of 600 m (facies 3, Fig. 6). Radiocarbon dating of mollusc shells found in these sediments yielded an age of 23, 550 ± 990 yr and therefore placed them in the LGM (Wiesner, 1993).
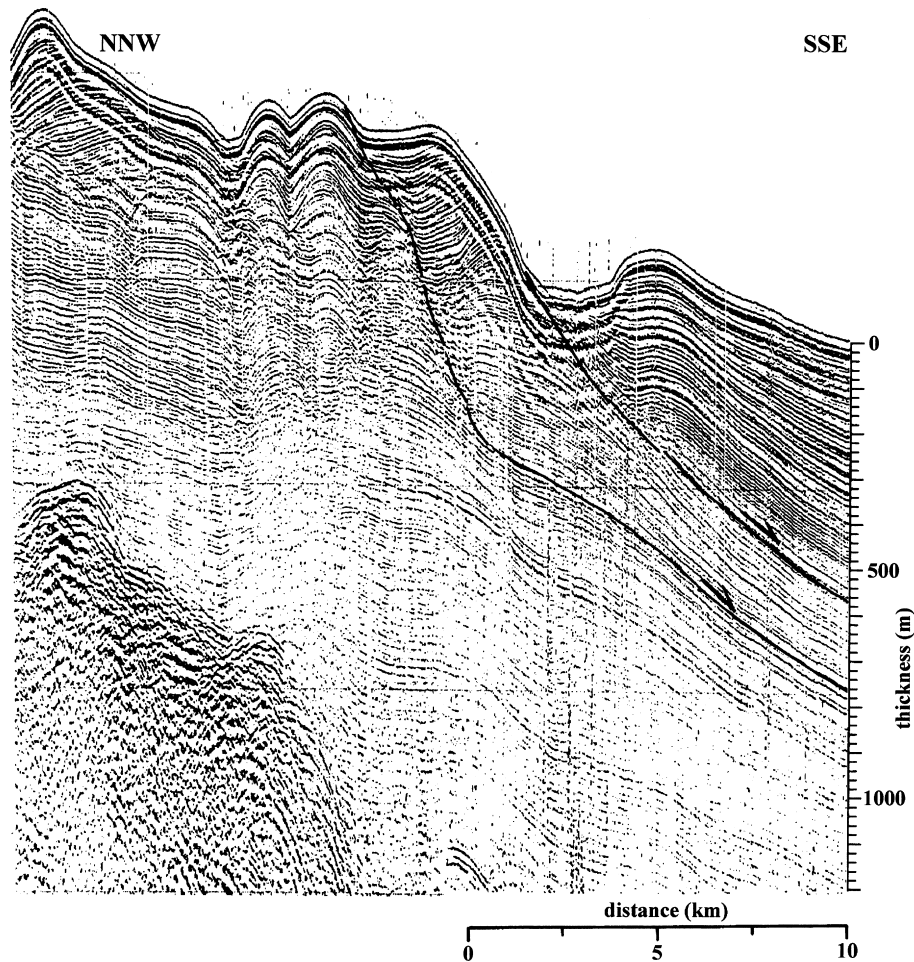
Fig. 12. Part of reflection seismic profile 19 (SO-95). Documented is the occurrence of recent slumping at the continental margin. See Fig. 3 for profile location.

Similar Pleistocene relict sediments occupy the upper slope around the Dongsha Islands where the Holocene is absent. Perhaps the Holocene cover here has been winnowed out by strong bottom currents. Evidence for this is provided by cross-bedding in box grab samples at 122 and 300 m water depths at stations 12 and 14 (Fig. 3), as well as by current measurements several km south of well LH 11-1-4 (Fig. 3) at depths of 60 and 320 m which yielded velocities of 60 and 30 cm/s, respectively (Sharma et al., 1991). In addition, analyses of core samples off Hong Kong show a distinct basinward increase in terrigenous components (Schönfeld and Kudrass, 1993), while sediment trap studies demonstrate that terrigenous material is transported in suspension over the shelf edge far into deep waters (Jennerjahn et al., 1992; Fig. 3). Mass wasting processes triggered by Recent tectonic movements (Lüdmann and Wong, 1999) dominate on the continental slope. Fig. 12 shows a sediment packet 730 m in thickness which has slid basinward (average $v_p = 2500$ m/s after Ludwig et al., 1979; Li, 1984). Additional evidence for mass movement can be seen on profile 1 (SO-50B, Fig. 7) on which a sediment slide on the slope that has glided basinward along a flat-lying seafloor-subparallel fault plane can be observed.

### 4.2. Middle slope-deepsea basin province

Fig. 13 shows a profile on the continental margin

off Hong Kong within the middle slope-deepsea province. Plotted on this figure are three sites of ODP Leg 184 drilled in the spring of 1999 (Wang et al., 2000). Site selection was based largely on our seismic profiles (Fig. 3). The primary objective of Leg 184 was to study the East Asian monsoon system from the rift stage of the South China Sea to Recent times. On the northern continental margin, drilling covered a time span back to the lower Oligocene (Wang et al., 2000). From the Pliocene to the Holocene, the carbonate concentration generally decreased, in particular since the mid-Pliocene. The past 3 Ma are characterised by high clastic sediment accumulation rates. A part of these clastic sediments was trapped in the course of their downslope transport in small basins which originated during the rift and post-rift stages (Lüdmann and Wong, 1999). The sedimentary cover of the slope ranges between 400 and >1000 m in thickness whereby the thickest accumulations are confined to these basins. The relief of the seafloor reflects the rough basement topography with horsts and grabens adjacent to one another in rapid succession. Sediment packets located at basin shoulders often slide downslope; these mass movements along the continental slope are presumably triggered by Recent tectonic movements.

Wang et al. (1999) discussed the Pleistocene–Holocene sedimentation regime on the continental slope based on four sediment cores from water depths of 1700 to 3400 m (cores 17937-2 to 17940-2; Fig. 3). They reported that the thickness of the Holocene decreases downslope from 6.5 to 1.1 m, while the sedimentation rate of the glacial section (LGM — isotope stage 3) increases from 19 cm/ka to 34–35 cm/ka (Wang et al., 1999). This increasing trend is accompanied by a (hemipelagic) fluvial component that increases downslope, and is attributed to: (1) a significant incision of the Pearl River during the LGM sea-level lowstand; and (2) transport of sediments discharged by the Pearl River downslope via canyons, leading to sediment bypass of the coring stations. However, our reflection seismic profiles show that during sea-level lowstands, the Peal River delta prograded to the shelf edge, and evidence for significant river downcutting or for the existence of major canyons is lacking. We suggest that the observed increase in fluvial sediments downslope may be a result of the location of their coring stations

which are downslope of the Dongsha Islands (Fig. 3). During the LGM, these islands were at a more elevated position than at present (see Section 5). The paleo-delta of the Pearl River was located more-or-less west of the Dongsha Islands, so that the fluvial sediment load reached only the more basinward-located coring stations; the supply of sediment to the upper slope stations was restricted by the uplifted Dongsha block.

Sediments of the deepsea basin within our study area have a total thickness of about 2 km. They can be divided into 14 seismic units (I–III, 1–11, Fig. 14). However, a correlation with the sequences on the continental shelf and slope is not possible because of the lack of drill hole data and the existence of a sharp structural boundary between these provinces. Nevertheless, the synrift units (sequence I–III, Table 4) can be readily separated seismo-stratigraphically from the post-rift units. Ke (1990) identified four unconformities ($T_g$, $T_4$, $T_2$ and $T_1$) in the deep basin, while Yao et al. (1994) recognised only two unconformities ($T_g$ and $T_2$; Table 1).

### 4.2.1. Cenozoic seismic units

The basinal deposits of the northern South China Sea are continuous and well-stratified. The stratigraphically oldest sediments occur in a small subbasin (Fig. 14C) which is separated from the continental slope by a basement ridge. Here, synrift deposits (I–III) overlie transitional crust. Within the adjacent subbasin that is underlain by oceanic basement, these units are missing (Fig. 14A). The sedimentary column consists of a succession of deepsea fans which were fed from different directions and which thin basinward. Some of the seismic units show lateral facies changes which probably correspond to transitions from the proximal to the distal part of a fan. For example, sequence 6 in profile 5 is dominated by discontinuous and locally chaotic reflectors of high amplitude (proximal fan, Fig. 14A), whereas the corresponding units in profile 7 are characterised by continuous reflectors of medium amplitude (distal fan, Fig. 14C).

### 4.2.2. Sedimentation processes

The succession of post-rift deposits reaches a thickness of 1855 m (average $V_p = 2200$ km/s, sonobuoy 126C17, Ludwig et al., 1979; Fig. 3, Table 3), implying an average computed sedimentation rate of 58 m/Ma
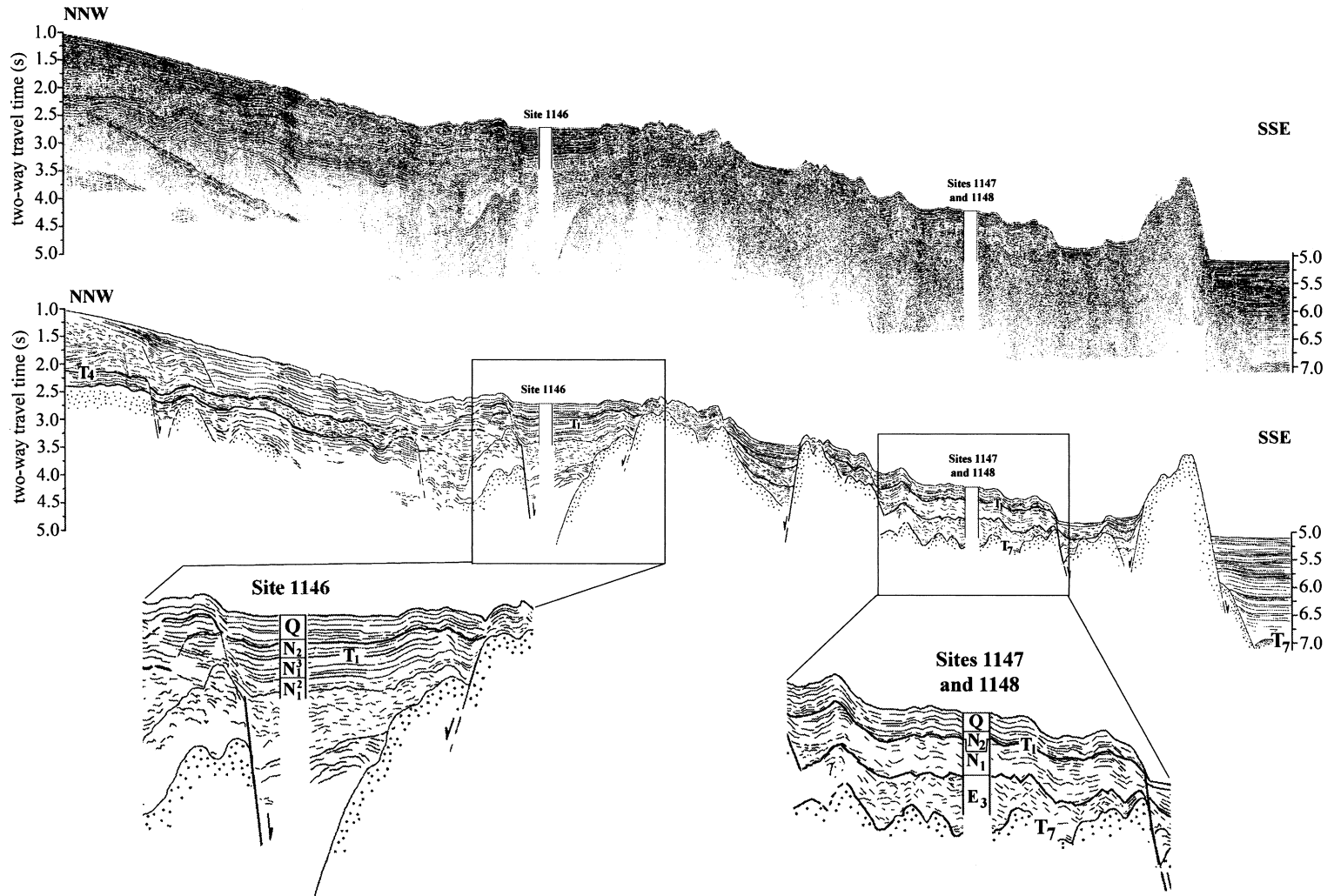
Fig. 13. (A) Part of reflection seismic profile 5 (SO-95) and (B) interpretation. Shown also is a correlation between the seismic stratigraphy and the stratigraphy of the ODP sites 1146-1148 after Wang et al. (2000). $T_1$, $T_4$ and $T_7$ are major unconformities (Tables 1 and 4). Q, Quaternary; $N_2$, Pliocene; $N_1^3$, upper Miocene; $N_1^2$, middle Miocene; $E_3$, Oligocene. See Fig. 3 for profile location.

since the beginning of seafloor spreading 32 Ma ago. This result is consistent with Plio-Pleistocene sedimentation rates of 38–60 m/Ma obtained at ODP site 1145 (water depth 3175 m, Wang et al., 2000; see Fig. 3 for site location). Studies on a sediment core retrieved from a water depth of 3766 m yielded an average Quaternary sedimentation rate of 104.5 m/Ma (SO-50B, core 29KL, Schönfeld and Kudrass, 1993; see Fig. 3 for core location). These values should be compared to typical biogenic pelagic sedimentation rates of 5–50 m/Ma and to average continental slope sedimentation rates of 10–200 m/Ma, respectively (Einsele, 1992). Thus, the deepsea basin of the northern South China Sea must have had a normal sediment supply over the past 32 Ma. In contrast, the subbasins of the Pearl River Mouth Basins (Zhu 1, Zhu 2 and Zhu 3) have higher sedimentation rates of 210, 290 and 230 m/Ma, respectively (Jin et al., 1984).

## 5. Neotectonics

The geological evolution of the Pearl River Mouth Basin, the main structural element of the continental margin of the northern South China Sea, can be divided into three main phases (Feng and Zheng, 1983; Jin et al., 1984; Su and He, 1987; Guong et al., 1989; Yu, 1994):

1. Basement rifting and basin subsidence from the upper Cretaceous to the early Oligocene;
2. Faulting, subsidence and filling of the subbasins from the late Oligocene to the early Miocene; and
3. Subsidence and filling of the entire basin since the middle Miocene.

After the cessation of seafloor spreading in the middle Miocene, two uplift events centered around the Dongsha Rise occurred in the northern South China Sea, namely at the Mio-/Pliocene boundary and during the Pleistocene (Lüdmann and Wong, 1999). After the major collision of Taiwan with the East China continental margin at the Mio-/Pliocene boundary (5 Ma ago), the NNW–WNW compression was transformed into a WSW–SSW strike–slip motion along the continental margin of the northern South China Sea. This transform motion, together with crustal stretching due to tensile forces of the subsiding oceanic crust and to subduction at the

Manila trench, generated a transtensional tectonic regime which activated and reactivated crustal zones of weakness and caused upwelling of mantle material, magma intrusion into the upper crust as well as uplift of the caprocks (Lüdmann and Wong, 1999).

Our seismo-stratigraphic interpretation of the reflection seismic profiles demonstrates that the study area can be divided into two regions which experienced different tectonic evolutions during the past ca. 630 ka, namely offshore Hong Kong and around the Dongsha Islands. For the zone off Hong Kong, a tectonics curve (Table 5) was reconstructed for the time interval from the lower Middle Pleistocene to the LGM (see Section 4.1.1). Although this curve should only be considered an order-of-magnitude estimate, it suggests that a subsidence phase that persisted till the lower Middle Pleistocene was succeeded by an uplift phase which lasted to the LGM. A comparison between our reconstructed regional relative sea-level curve and that published by Xue et al. (1996) shows that a lower Middle to Late Pleistocene uplift event cannot be recognised at the more landwardly-located well ZQ3 (Fig. 3). This probably implies that the uplift was differential and that its amplitude increased basinward.

Lowstand wedges near the shelf edge off Hong Kong occurring today at depths not explicable by eustatic sea-level changes alone document the importance of the role of regional tectonics in deltaic sedimentation here from the Pliocene to the Holocene (see Section 4). On the continental margin around the Dongsha Islands, however, a different sedimentary regime dominated. Box grab samples and our seismic profiles show that on the Dongsha Rise, the Pliocene section and a large part of the Pleistocene strata are missing. Seismic profile 16 (SO72-A, Fig. 4) shows northward-dipping Miocene layers overlain by a thin sheet of Pleistocene relict sand (grab sample and Parasound data). The Miocene age assignment is based on correlation with the lithostratigraphy of well LH 11-1-1A (Fig. 3, Table 2) (Lüdmann and Wong, 1999), while the surficial relict sands were sampled with a box grab and their extent traced to a water depth of 600 m (facies 3a and 3b, Fig. 6). The fossils from these sands, consisting mostly of mollusc shells, are from the LGM (Wiesner, 1993). We note that these relict sands do not show any sign of redeposition, and that the Pliocene to Pleistocene strata terminate by offlap against (and are therefore truncated by) them
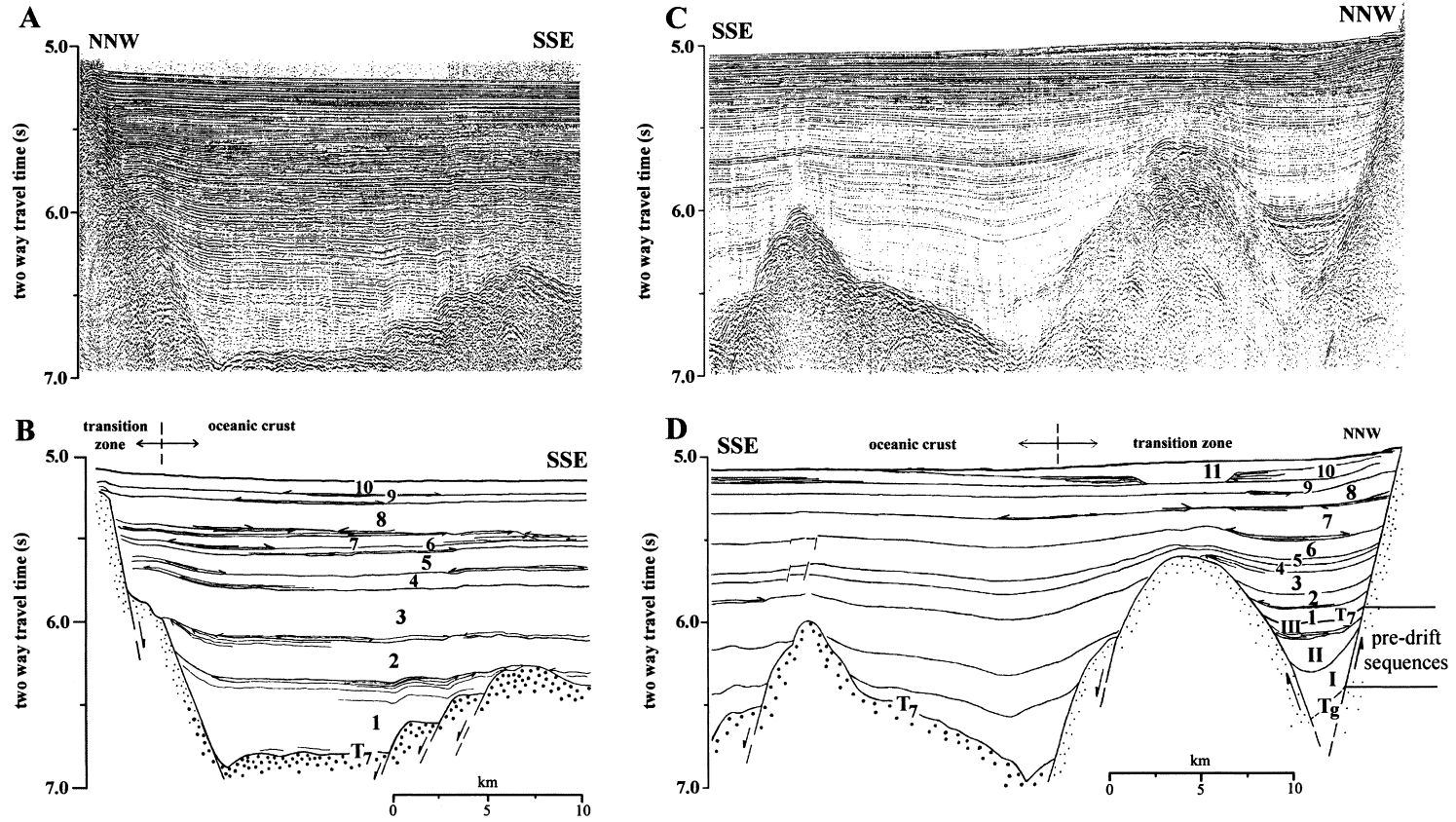
Fig. 14. (A) Part of reflection seismic profile 5 (SO-95) and (B) interpretation. This profile shows the seismic units 1–10 (see text for explanation) and the major unconformity $T_7$ (see Tables 1 and 4). (C) Part of reflection seismic profile 7 (SO-95) and (D) interpretation. This profile shows the seismic units 1–11 (see text for explanation) and the major unconformities $T_7$ and $T_g$ (see Tables 1 and 4). See Fig. 3 for profile locations.

(Fig. 4). Fig. 2 gives the distribution of the Pliocene and Miocene formations after the Quaternary is back-stripped. It suggests two possible scenarios. The first and more likely is that during the Pleistocene, the entire Dongsha Rise was uplifted and subaerially exposed, and erosion of the uppermost strata occurred (submarine redeposition of this extent seems unlikely). Our high-resolution PARASOUND profile 11 farther to the east is consistent with this view (Figs. 3 and 5). Miocene strata that outcrop at the SSE end of this profile are covered by relict sediments marked by sharp, prolonged surface reflections with few or no surface-parallel subbottom echoes. The thickness of these relict sediments reaches 10–15 m. Although their top was dated to be at the LGM, the age of the bottom (a lower limit for the age of uplift) is unknown because the box grab penetrated only the first meter of the seafloor. The Pleistocene mollusc fauna of these relict sediments points to a maximum paleo-water depth of ca. 100 m. Because the late Pleistocene sea-level fall was ca. 130 m and the present-day maximum depth of occurrence of these sediments is 600 m (facies 3a and 3b, Fig. 6), the Dongsha Rise must have subsided about 370 m since the LGM. This gives a calculated average subsidence rate of around 15 m/ka, an extremely high rate but one which applies only to the past 24 kyr. The subsidence is presumably differential, its rate increasing from the shelf edge to the middle slope. The alternative scenario is that these relict sediments are a result of mass wasting and sediment reworking. Although significant mass movements on the Dongsha Rise within the water depth range of 200–600 m have not been observed, their existence cannot be completely ruled out. More studies are necessary to distinguish between these two possible interpretations.

Additional indirect evidence for uplift of the Dongsha Rise is provided by the ODP drill holes. Wang et al. (2000) reported that there was a significant increase in the supply of terrestrial material 3 and 0.25 Ma ago. We suggest that these two sedimentation events may have been related to the uplift episodes of the Dongsha Rise, which resulted in its subaerial exposure and rapid erosion. The erosional products must have been transported downslope to the adjacent ODP sites.

## 6. Conclusions

A sequence stratigraphic interpretation of high-resolution reflection seismic profiles on the northern continental margin of the South China Sea led to the recognition of four type 1 sequences for the past 690 kyr. These sequences are a result of high-frequency sea-level fluctuations of the 4th order. They consist of lowstand systems tracts of a prograding shelf edge delta deposited during a relative sea-level fall, and are bounded by polygenetic surfaces representing phases of regression, transgression as well as sea-level stillstand. Internal discontinuities within the prograding delta complexes may be attributed to minor sea-level changes of the 5th order or to delta lobe switching. A preliminary correlation of the relative sea-level curve for the continental margin off Hong Kong deduced from our seismic data with the SPECMAP oxygen isotope curve suggests that the position of the regressive units through time are largely controlled by neotectonics and eustatic sea-level change. Studies on Quaternary sediments around Hong Kong in which 4th order sea-level fluctuations and minor changes of the 5th order have been recognised support our seismo-stratigraphic interpretation (Fyfe et al., 1997; Yim, 1999). Thus, the 4th order fluctuations studied (which correspond to our regressive units A, B and D) cover >440 kyr and are characterised by terrestrial sedimentation combined with subaerial fluvial erosion. Each 4th order cycle consists of minor sea-level changes of higher order which are also documented in our seismic records.

In contrast to the continental margin south of Hong Kong, the region around the Dongsha Islands has a Pliocene–Quaternary sedimentation history dominated by uplifts accompanied by widespread subaerial exposure of parts of the Dongsha Rise. This led to erosion of the Pliocene and much of the Pleistocene strata. We postulate that these uplifts are due to magmato-tectonic events related to the collision between Taiwan and the East Asian continent (Lüdmann and Wong, 1999). Thermal subsidence since the LGM proceeds at a rate averaging 15 m/ka. We note that the occurrence of relict sands down to a present-day water depth of 600 m could have also resulted from mass wasting and sediment reworking rather than subsidence.

The Recent depositional environment is characterised by sediment accumulation within the river estuaries as well as by transport of terrigenous material to the deepsea basin which remains uninterrupted

in spite of the Holocene sea-level rise. The mass wasting processes predominant on the continental slope are controlled largely by tectonic triggering and over-steepening. Sediments within the deepsea basin are over 2 km in thickness and may be subdivided into fourteen depositional units that cover the rift and post-rift phases.

## Acknowledgements

## References

British Hydrographic Office, 1986. China Sea-Northern Portion-Eastern Sheet. London. Scale 1:1,500,000.

Cai, D.Q., 1987. A preliminary analysis of hydrocarbon exploration of Dongsha massif. In: Collection of Papers from the International Petroleum Geological Convention, Northern South China Sea Continental Shelf, China. China Oil Magazine (Hong Kong), pp. 439–455.

Chen, S., Hu, P., 1989. Tertiary reef complexes in the Zhujiangkou (Pearl River Mouth) Basin and their significance for hydrocarbon exploration. China Earth Sci. 1 (1), 21–29.

Chen, J., Xu, S., Sang, J., 1994. The depositional characteristics and oil potential of the paleo-Pearl River delta system in the Pearl River Mouth Basin, South China Sea. Tectonophysics 235, 1–11.

Chen, S., Li, Z., 1987. Major oil accumulation characteristics and exploration direction in the Pearl River Mouth Basin. In: Collection of Papers from the International Petroleum Geological Convention, Northern South China Sea Continental Shelf, China. China Oil Magazine (Hong Kong), pp.12–23.

Damuth, J.E., 1980. Quaternary sedimentation processes in the South China Basin as revealed by echo-character mapping and piston-core studies. In: Hayes, D.E. (Ed.), The Tectonic and Geologic Evolution of Southeast Asian Seas and Islands. Part 1. American Geophysical Union Geophysical Monograph 23, 105–125.

Diaz, J.I., Maldonado, A., 1990. Transgressive sand bodies on the Maresme continental shelf, western Mediterranean Sea. Mar. Geol. 91, 53–72.

Einsele, G., 1992. Sedimentary Basins. Springer, Berlin/Heidelberg, 628 pp.

Emery, K.O., Niino, H., Sullivan, B., 1970. Post-Pleistocene levels of the East China Sea. In: Turekian, K.K. (Ed.), Late Cenozoic Glacial Ages. Yale University Press, New Haven, pp. 381–390.

Erlich, R.N., Barrett, S.F., Guo, B.J., 1990. Seismic and geologic characteristics of drowning events on carbonate platforms. Am. Assoc. Pet. Geol. Bull. 74 (10), 1523–1537.

Feng, W., Shi, Y., 1997. Coastal remnants of the last glacial age on the continental shelf of the northern South China Sea. In: Jablonski, N.G., (Ed.), The Changing Face of East Asia during the Tertiary and Quaternary. Proceedings of the Fourth Conference on the Evolution of the East Asian Environment, pp. 150–155.

Feng, W., Xue, W., Yang, D., 1988. The Geological Environment of the Late Quaternary in the Northern South China Sea. Guangdong Science and Technology Publishing House, 261 pp (in Chinese).

Feng, Z., Miao, W., Zheng, W., Chen, S., 1992. Structure and hydrocarbon potential of the para-passive continental margin of the northern South China Sea. In: Watkins, J.S., Feng, Z., McMillen, K.J. (Eds.), Geology and Geophysics of Continental Margins. Am. Assoc. Pet. Geol., Mem. 53, 27–41.

Feng, Z., Zheng, W., 1983. Tectonic evolution of Zhujiangkou (Pearl River Mouth) Basin and origin of South China Sea. Acta Geol. Sin. 3, 212–222 (in Chinese).

Fulthrope, C.S., Schlanger, S.O., 1989. Paleo-oceanographic and tectonic settings of early Miocene reefs and associated carbonates of offshore Southeast Asia. Am. Assoc. Pet. Geol. Bull. 73 (6), 729–756.

Fyfe, J.A., Selby, I.C., Shaw, R., James, J.W.C., Evans, C.D.R., 1997. Quaternary sea-level change on the continental shelf of Hong Kong. J. Geol. Soc. London 154, 1031–1038.

Gu, Q., Rao, K., Li, X., Xu, X., Wang, J., Zhu, Q., 1990. Remote Sensing Application in Lingdingyang Estuary. Chinese Science Press, Beijing (in Chinese).

Guan, B., 1993. Winter counter-wind current off the southeastern China coast and preliminary investigation of its source. In: Su, J., Wen-Sin, C., Ya, H. (Eds.), Proceedings of the Symposium on the Physical and Chemical Oceanography of the China Seas. China Ocean Press, pp. 1–9.

Guong, Z., Jin, Q., Qiu, Z., Wang, S., Meng, J., 1989. Geology, tectonics and evolution of the Pearl River Mouth Basin. In: Zhu, X. (Ed.), Chinese Sedimentary Basins. Elsevier, Amsterdam, pp. 181–196.

Hu, P., Xie, Y, 1987. Tertiary reef complexes and their relationship to hydrocarbon accumulation in Pearl River Mouth Basin. In: Collection of Papers from the International Petroleum Geological Convention, Northern South China Sea Continental Shelf, China. China Oil Magazine (Hong Kong), pp. 505–527.

Huang, J., Song, C., 1981. A richly endowed coastal zone. Renmin Huabao 11, 1–5 (in Chinese).

Imbrie, J., Berger, A., Boyle, E.A., Clemens, S.C., Duffy, A., Howard, W.R., Kukla, G., Kutzbach, J., Martinson, D.G., McIntyre, A., Mix, A.C., Molfino, B., Morley, J.J., Peterson, L.C.,

Pisias, N.G., Prell, W.L., Raymo, M.E., Shackleton, N.J., Toggweiler, J.R., 1993. On the structure and origin of major glaciation cycles. 2: the 100,000-year cycle. Paleoceanography 8 (6), 699–735.

Jennerjahn, T.C., Liebezeit, G., Kempe, S., Xu, L., Chen, W., Wong, H.K., 1992. Particle flux in the northern South China Sea. In: Jin, X., Kudrass, H.-R., Pautot, G. (Eds.), Marine Geology and Geophysics of the South China Sea. Proc. Symp. Recent Contributions to the Geological History of the South China SeaChina Ocean Press, Hangzhou, pp. 228–235.

Jin, Q., Zeng, W., Zhong, S., Wu, Z., 1984. Analysis on petroleum geological conditions of the Pearl River Mouth Basin. Acta Geol. Sin. 4, 324–336 (in Chinese).

Ke, C., 1990. Features of seismic stratigraphy and development of sedimentary sequence in the central basin of the South China Sea. In: Jin, X., Kudrass, H.-R., Pautot, G. (Eds.), Marine Geology and Geophysics of the South China Sea. Proc. Symp. Recent Contributions to the Geological History of the South China SeaChina Ocean Press, Hangzhou, pp. 92–100.

Lee, T.-Y., Lawver, L.A., 1995. Cenozoic plate reconstruction of Southeast Asia. Tectonophysics 251, 85–138.

Li, C., Chen, G., Yao, M., Wang, P., 1991. The influence of suspended load on sedimentation in the coast zones and continental shelves of China. Mar. Geol. 96, 341–352.

Li, P., Rao, C., 1994. Tectonic characteristics and evolution history of the Pearl River Mouth Basin. Tectonophysics 235, 13–25.

Li, Z.-W., 1984. A discussion on the crustal nature of the central and northern parts of the South China Sea. Acta Geophys. Sin. 27 (2), 153–166 (in Chinese with English abstract).

Lüdmann, T., Wong, H.K., 1999. Neotectonic regime on the passive continental margin of the northern South China Sea. Tectonophysics 311, 113–138.

Ludwig, W.J., Kumar, N., Houtz, R.E., 1979. Profiler-sonobuoy measurements in the South China Sea basin. J. Geophys. Res. 84 (B7), 3505–3518.

Niino, H., Emery, K.O., 1961. Sediments of shallow portions of East China Sea and South China Sea. Geol. Soc. Am. Bull. 72, 731–762.

Pautot, G., Rangin, C., Briais, A., Tapponnier, P., Beuzart, P., Lericolais, G., Mathieu, X., Wu, J., Han, S., Li, H., Lu, Y., Zhao, J., 1986. Spreading direction in the central South China Sea. Nature 321, 150–154.

Penland, S., Boynd, R., Suter, J.R., 1988. Transgressive depositional systems of the Mississippi delta plain: a model for barrier shoreline and shelf development. J. Sediment. Petrol. 58, 932–949.

Posamentier, H.W., Allen, G.P., James, D.P., Tesson, M., 1992. Forced regressions in a sequence stratigraphic framework: concepts, examples, and exploration significance. Am. Assoc. Pet. Geol. Bull. 76 (11), 1687–1709.

Posamentier, H.W., Vail, P.R., 1988. Eustatic controls on clastic deposition II — sequence and systems tract models. In: Wilgus, C.K., Hastings, B.S., Kendall, C.G.St.C., Posamentier, H.W., Ross, H.C.A., Van Wagoner, J.C. (Eds.), Sea Level Changes — An Integrated Approach. Soc. Econ. Paleontol. Mineral. Spec. Publ. 42, 125–154.

Posamentier, H.W., Jervey, M.T., Vail, P.R., 1988. Eustatic controls on clastic deposition I — conceptual framework. In: Wilgus, C.K., Hastings, B.S., Kendall, C.G.St.C., Posamentier, H.W., Ross, H.C.A., van Wagoner, J.C. (Eds.), Sea Level Changes — An Integrated Approach. Soc. Econ. Paleontol. Mineral. Spec. Publ. 42, 109–124.

Ru, K., Pigott, J.D., 1986. Episodic rifting and subsidence in the South China Sea. Am. Assoc. Pet. Geol. Bull. 70 (9), 1136–1155.

Sangree, J.B., Widmier, J.M., 1977. Seismic stratigraghy and global changes of sea level. Part 9: seismic interpretation of clastic depositional facies. In: Payton, C.E. (Ed.), Seismic Stratigraphy — Applications to Hydrocarbon Exploration. Am. Assoc. Pet. Geol., Mem. 26, 165–184.

Sarnthein, M., Wang, P. (Eds.), 1999. Response of the West Pacific Marginal Seas to Global Climate Change. Marine Geology Special Issue 159, 304 pp.

Schönfeld, J., Kudrass, H.-R., 1993. Hemipelagic sediment accumulation rates in the South China Sea related to late Quaternary sea-level changes. Quat. Res. 40, 368–379.

Sharma, J.N., Mu, S., Soeraas, P.-E., 1991. 18 months of metocean measurements in the Pearl River basin block 29/04 in the South China Sea. 23rd Annual Offshore Technology Conference Transactions, pp. 391–402.

Shaw, P.-T., Chao, S.-Y., 1994. Surface circulation in the South China Sea. Deep-Sea Res. 41, 1663–1683.

SCSIO (South China Sea Institute of Oceanology) (Ed.), 1986. Map of the Seafloor Morphology of the South China Sea. Scale 1:3,000,000. Geological Maps Press.

Spangler-Nissen, S., Hayes, D.E., Buhl, P., Diebold, J., Yao, B., Zeng Weijun, Chen, Y., 1995. Deep penetration seismic soundings across the northern margin of the South China Sea. J. Geophys. Res. 100 (B11), 22 407–22 433.

Su, N., He, Z., 1987. The characteristics of fault activities in the Pearl River Mouth Basin and their control of hydrocarbons. In: Collection of Papers from the International Petroleum Geological Convention, Northern South China Sea Continental Shelf, China. China Oil Magazine (Hong Kong), pp. 191–216.

Sydow, J., Roberts, H.H., 1994. Stratigraphic framework of the Late Pleistocene shelf-edge delta, northeast Gulf of Mexico. Am. Assoc. Pet. Geol. Bull. 78 (8), 1276–1312.

Taylor, B., Hayes, D.E., 1980. The tectonic evolution of the South China Basin. In: Hayes, D.E. (Ed.), The Tectonic and Geologic Evolution of Southeast Asian Seas and Islands, Part 1. American Geophysical Union Geophysical Monograph 23, 89–104.

Taylor, B., Hayes, D.E., 1983. Origin and history of the South China Sea basin. In: Hayes, D.E. (Ed.), The Tectonic and Geologic Evolution of Southeast Asian Seas and Islands, Part 2. American Geophysical Union Geophysical Monograph 27, 23–56.

Tesson, M., Allen, G.P., Ravenne, C., 1993. Late Pleistocene lowstand wedges on the Rhône continental shelf. Spec. Publ. Intl Assoc. Sediment. 18, 183–196.

Tesson, M., Posamentier, H.M., Gensous, B., 1999. Stratigraphic organisation of Late Pleistocene deposits of the western part of the Golfe du Lion shelf (Languedoc shelf), western Mediterranean Sea, using high-resolution seismic and core data. Am. Assoc. Pet. Geol. Bull. 84 (1), 119–150.

Tyrrell, W.W., Christian, H.E., 1992. Exploration history of Liuhua

11-1 field, Pearl River Mouth basin, China. Am. Assoc. Petr. Geol. Bull. 76 (8), 1209–1223.

Vail, P.R., Mitchum Jr., R.M., Thompson, S., 1977. Seismic stratigraphy and global changes of sea level. Part 3: relative changes of sea level from coastal onlap. In: Payton, C.E. (Ed.), Seismic Stratigraphy — Applications to Hydrocarbon Exploration. Am. Assoc. Pet. Geol. Mem. 26, 63–81.

Wang, L., Sarnthein, M., Erlenkeuser, H., Grimalt, J., Grootes, P., Heilig, S., Ivanova, E., Kienast, M., Pelejero, C., Pflaumann, U., 1999. East Asian monsoon climate during the Late Pleistocene: high-resolution sediment records from the South China Sea. Mar. Geol. 156, 245–284.

Wang, P., Prell, W.L., Blum, P., et al., 2000. Exploring the Asian monsoon through drilling in the South China Sea. Proceedings of the Ocean Drilling Program: Initial Report 184, 1–77.

Wang, P., Sarnthein, M., Wang, L., Jian, J., Xu, Z., Zheng, L., Luo, Y., Xia, K., Xu, D. Wong, H.K., Lüdmann, T., Kuhnt, W., 1996. East Asian monsoon history as recorded in the South China Sea and its global climate impact. Revised ODP proposal 484, Laboratory of Marine Geology, Tongji University, 60 pp. (unpublished).

Wang, P., Wang, L., Bian, Y., Jian, Z., 1995. Late Quaternary paleoceanography of the South China Sea: surface circulation and carbonate cycles. Marine Geology 127, 145–165.

Wiesner, M.G., 1993. Sedimentary facies and organic matter characteristics of the northern continental margin of the South China Sea. In: Wong, H.K., (Editor), Quaternary Sedimentation Processes in the South China Sea, R/V *Sonne*, Cruise SO-72A. BMBF, Germany, Final Report, 78-122 (unpublished).

Wu, J., 1988. Cenozoic basins of the South China Sea. Episodes 11 (2), 91–96.

Wu, J., 1994. Evaluation and models of Cenozoic sedimentation in the South China Sea. Tectonophysics 235, 77–98.

Xue, W., Zheng, Z., Zhan, H., Lei, Y., 1996. In: Liu, Q., Chen, B., Xu, M., Kou, Y. (Eds.), Sea-level environmental changes during the Quaternary in the northern South China Sea. Collections of Paper on Marine Geology and Geophysics, 1–12. Qingdao Ocean University Press (in Chinese).

Yao, B., Zeng, W., Hayes, D., Spangler, S., 1994. The Geological Memoir of South China Sea Surveyed Jointly by China and USA. China University of Geosciences Press (204 pp.; in Chinese with English abstract).

Yim, W.W.-S., 1999. Radiocarbon dating and the reconstruction of late Quaternary sea-level changes in Hong Kong. Quat. Intl 55, 77–91.

Yu, H.S., 1994. Structure, stratigraphy and basin subsidence of Tertiary basins along the Chinese southeastern continental margin. Tectonophysics 253, 63–76.